DØNote XXXX - Draft v0.23

DØ Search for Stopped Gluinos using p14 Data

Andrew Haas [1]

1. Columbia University / Nevis Labs – USA

March 9, 2006

Abstract

A long-lived gluino is a generic prediction of several models of beyond the Standard Model physics, such as Split-SUSY. Some fraction of the hadronized gluinos (R-hadrons) can lose enough momentum to come to rest in the calorimeters. About 350 pb^{-1} of Run II data reconstructed with p14 software is analyzed in search of stopped gluinos decaying into a jet and a neutralino. No excess is observed above the expected background from cosmic-muon induced showers, and limits are placed on the stopped gluino cross-section as a function of the gluino and neutralino masses.

1 Introduction and Theory

Split-Supersymmetry is a relatively new variant of Supersymmetry, in which the Supersymmetric scalars are heavy (possibly GUT-scale) compared to the (SUSY) fermions [1]. This simple relaxation of one of the foundations of standard Supersymmetry avoids many fine-tunings which must be incorporated to remain consistent with observations while still preserving the favored consequences. A dark-matter candidate is still present in the theory to explain the observed cold-dark matter density in the Universe, GUT-scale coupling unification still occurs, and the required Supersymmetry is still present as needed for String theory. Due to the scalars' high masses, the gluino decays (into squarks and the neutralino LSP) are suppressed, and the gluino lifetime is determined by this SUSY-scalar mass scale (M_{SUSY}). The gluinos have time to hadronize into "R-hadrons" [1], colorless bound states of a gluino and other quarks or gluons.

At the Tevatron, R-hadrons could be pair produced through strong interactions. If $M_{SUSY} > 10^6 GeV$, which is likely, since the natural M_{SUSY} is the GUT scale, the R-hadrons live long enough ($> 10ns$) to reach the DØ calorimeters. Hadronization models of gluinos [2] predict a spectrum with degenerate light meson-like states, leading to a fraction of R-hadrons which are electrically charged of about 1/2. R-hadrons can also become charged when passing through matter. As studied in [3], some charged R-hadrons can become "stopped gluinos", by losing all of their momentum through ionization and coming to rest in the calorimeters. Most of these stopped gluinos would later decay into a jet (from a gluon) and a neutralino (LSP).

This analysis searches for stopped gluinos (G) produced at the Tevatron in Run II, decaying into a jet plus neutralino. The stopped gluino lifetime is assumed to be long enough such that the decay of the gluino occurs during a bunch-crossing adequately later than the one which produced it (about $10\mu s$). The decay is also assumed to take place soon enough such that data is consistently being recorded during the decay, a limit of about 1 hour [2]. (The data is almost always being recorded during the gluino production.) Since the decay most likely occurs during a bunch-crossing with very little other high-p_T activity, the signal signature is a largely empty event with a single high-p_T jet and thus large missing E_T.

It is worth noting that several other interesting and more complicated related signatures are also available. When one of the pair-produced gluinos stops in the calorimeters, 30% of the time the other one stops as well [3], since the p_T of the two gluinos are highly correlated in each event. This makes possible the search for "double-bang" events, where two decays are observed close in time. These could be a way to directly measure the gluino lifetime and thus M_{SUSY}. Another phenomenon is the two-jet decay plus MET, coming from the decay $G \to q\overline{q}\chi_1^0$, which may be possible to distinguish from the single-jet decay. The branching fraction of double- to single- jet decays would also provide information on M_{SUSY}. Finally, it may be possible to observe the decay $G \to \chi_2^0 j \to \chi_1^0 \mu^+ \mu^- j$ with two muons coming from the jet location with an invariant

[1] They are called "R-hadrons" because they are only long-lived if R-parity is conserved, in which SUSY particles have opposite R-parity from Standard Model particles.

[2] In many models, and particularly for gluinos >500 GeV, Big-Bang nucleosynthesis constrains the gluino lifetime to be <100 seconds, but lighter gluinos could live up to 100,000 years.

mass less than or equal to the mass difference of the two neutralinos. However, the search for and study of these processes will be left to future investigations.

2 Simulation

The stopped gluino decays a majority of the time into a gluon plus a neutralino (LSP). There is also some branching fraction to 2 quarks plus a neutralino, possibly up to 50% depending on various model parameters, but these decays will be ignored and the analysis specifically searches for mono-jet events (i.e. limits will be set on the cross-section x BR to a gluon). The radial location of the gluino when it decays depends on the way the gluinos lose energy via ionization and stop in the calorimeters. This calculation was performed [3] for a distribution of material similar to the DØ calorimeters (production at the Tevatron). The $|\eta|$ distribution is determined by the fact that gluinos would tend to be produced near threshold at the Tevatron, and that only slow gluinos would stop. Therefore the gluinos are expected to be distributed proportional to $\cos\theta$, with more than 75% of gluinos stopping in $|\eta|<1$. (This can be understood as being due to the fact that gluinos produced centrally will have smaller total momenta, since p_z is small.) The gluinos are randomly oriented in space when they decay, thus the gluon is emitted in a random direction. The energy of the gluon (jet) depends on the gluino and LSP masses:

$$E = (M_g^2 - M_{LSP}^2)/2M_g \tag{1}$$

To simulate the jets that would be produced by stopped gluino decays, Pythia was used to produce Z+gluon events (MSEL=13) with the Z forced to decay to neutrinos. The location of the interaction point (the gluino decay location) was set to (x,y,z)=(0±20,120±20, 0±80) cm, near the outside of the EM calorimeter layers, by overwriting the mcvertex.rcp file. The vertex is chosen in each event according to a Gaussian distribution in each coordinate. The 80 cm RMS of the z vertex location roughly corresponds to the $|\eta|$ distribution of the stopped gluinos, but events are further weighted such that the final events are proportional to $\tanh\eta = \cos\theta$, as expected for stopped gluinos. Initial-state radiation (ISR) was switched off in Pythia, and so were multiple parton interactions, since we do not really want to simulate a full $p\overline{p}$ beam. The $|\eta|$ of the gluon was restricted to be less than 0.1 at the generator level. This $|\eta|$ cut prevents the gluon jet from obtaining extra energy from the boost of the system along the beam direction. The spectator particles coming from the rest of the $p\overline{p}$ interaction, such as the underlying event, were removed at the generator stage by stopping (setting momenta to 0.01) all particles with $|pz/E| > 0.95$. Finally, a random 3D rotation was applied to the remaining particles, to simulate the random decay axis of the gluino.

4 samples of "stopped gluino MC" were privately produced using release p14.07.00 (and p14.06.01 for DØReco), containing 1000 events each. The samples had mass cuts at the generator level [3], of 195-205, 295-305, 395-405, and 495-505 GeV, corresponding

[3] CKIN(1)-(2) in Pythia

to gluino masses of about 200, 300, 400, and 500 GeV, respectively, for an LSP mass of 90 GeV (the Z behaves similarly to an LSP of the same mass). Using Equation 1, we note that these samples thus correspond to generated parton (jet) energies of 80, 137, 190, and 242 GeV, respectively. A little more than half the gluino energy goes to the LSP. Plots of the simulated gluino jets are shown in Figure 1, for jet energy, n90 (number of towers needed to make up 90% of the jet E_T), ϕ, η, ϕ-width (the E_T-weighted RMS of the jet towers' ϕ), and η-width (the E_T-weighted RMS of the jet towers' η). Some event displays of simulated events made with the d0ve program are shown in Figures 2 - 6.

3 Data Sample

Data taken from November 2002 – August 2004, about 350 pb^{-1}, were reconstructed and corrected with the p14.03.01 – p14.06.01 versions of the reconstruction software, and corrected with "PASS2" software. Since no $p\overline{p}$ beam-interaction is expected to be correlated with the stopped gluino decay, the "DIFF" skim was selected and one of the "GAPSN" triggers were required for each event. (Of course, minimum-bias interactions can occur during the same bunch crossing as the decay, and efficiency corrections will be made for this. The "QCD" skim with the JT125_TT trigger required was used for studying the efficiency of the GAPSN trigger requirement.)

The GAPSN triggers require no firing of either the North or South luminosity counters, placed on the front face of the end-cap calorimeters at high $|\eta|$. Two versions exist, the first (JT_15TT_GAPSN) has lower calorimeter thresholds and is prescaled at some very high luminosities, and the second (JT_45TT_GAPSN) is always un-prescaled. The first trigger requires 2 L1 calorimeter towers above 3 GeV and a 15 GeV L3 jet. The second requires 2 L1 calorimeter towers above 5 GeV and a 45 GeV L3 jet. Each event is required to have fired one of these two triggers. About 7.9 million events exist in the initial trigger-selected, skimmed, data sample. This corresponds to a data rate of about 0.5 Hz.

4 Object Identification

Jets were reconstructed with the Run II Improved Legacy Cone Algorithm (ILCA) [4] with cone size of 0.5 (JCCB). The T42 hot-cell killing algorithm was used during reconstruction, as for all of PASS2. Jets were not required to pass any quality criteria. Jet energies were not corrected back to the particle level for detector and physics effects using any jet energy scale factors, since the assumptions used to derive these corrections (a projective geometry, etc.) are no longer valid for these jets.

Muons were reconstructed and no extra quality criteria or corrections were applied. They were separated by their number of "segments" (NSEG) as 1, 2, or 3. Muons with NSEG=1 are A-layer only muon segments, whereas the other muons also have matching segments in the B/C layers, outside the iron toroid. No inner-track match was required for the muons, and no timing cuts were applied.

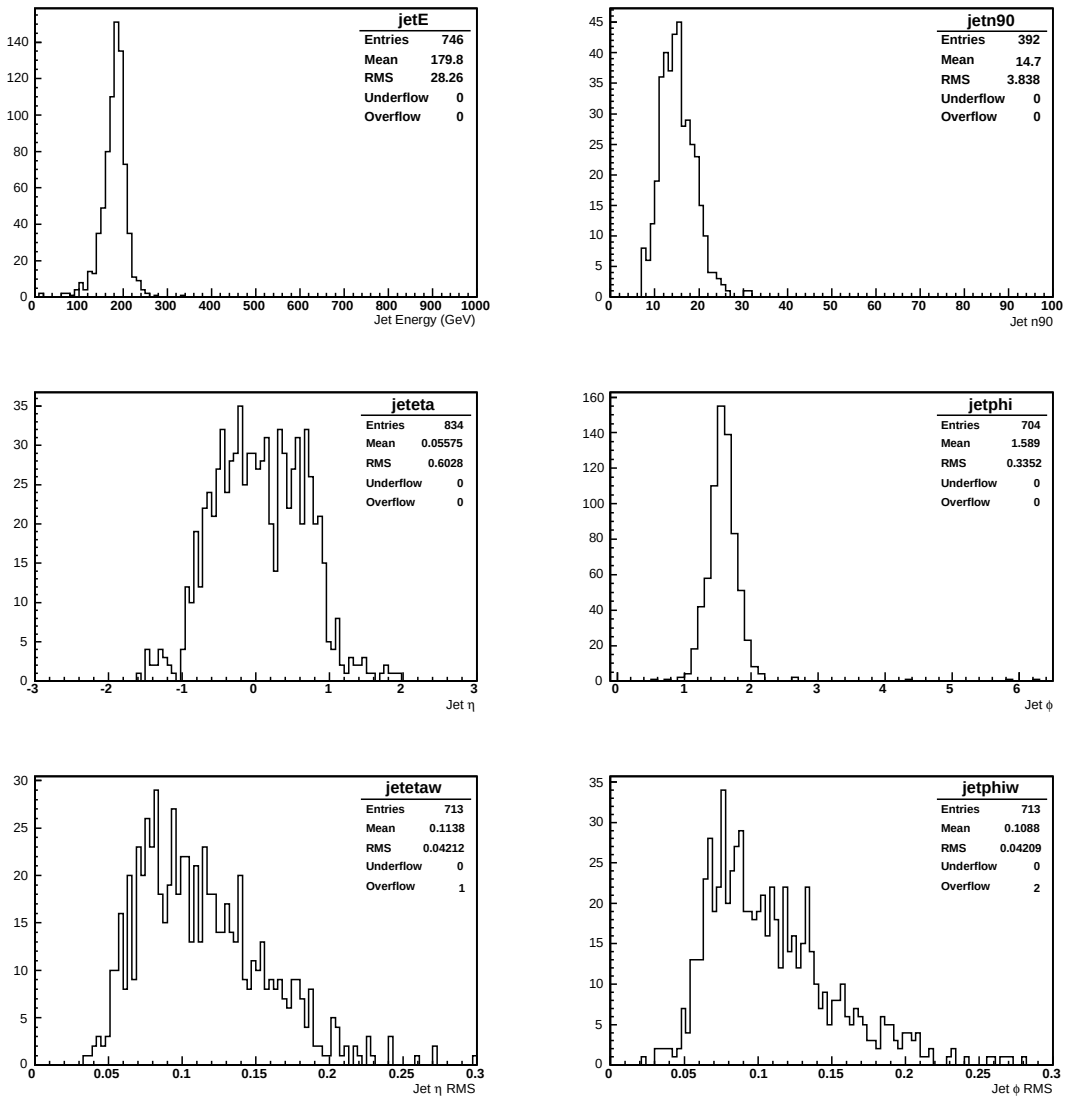

Figure 1: The jet properties for the m_G=400 GeV simulated MC sample.

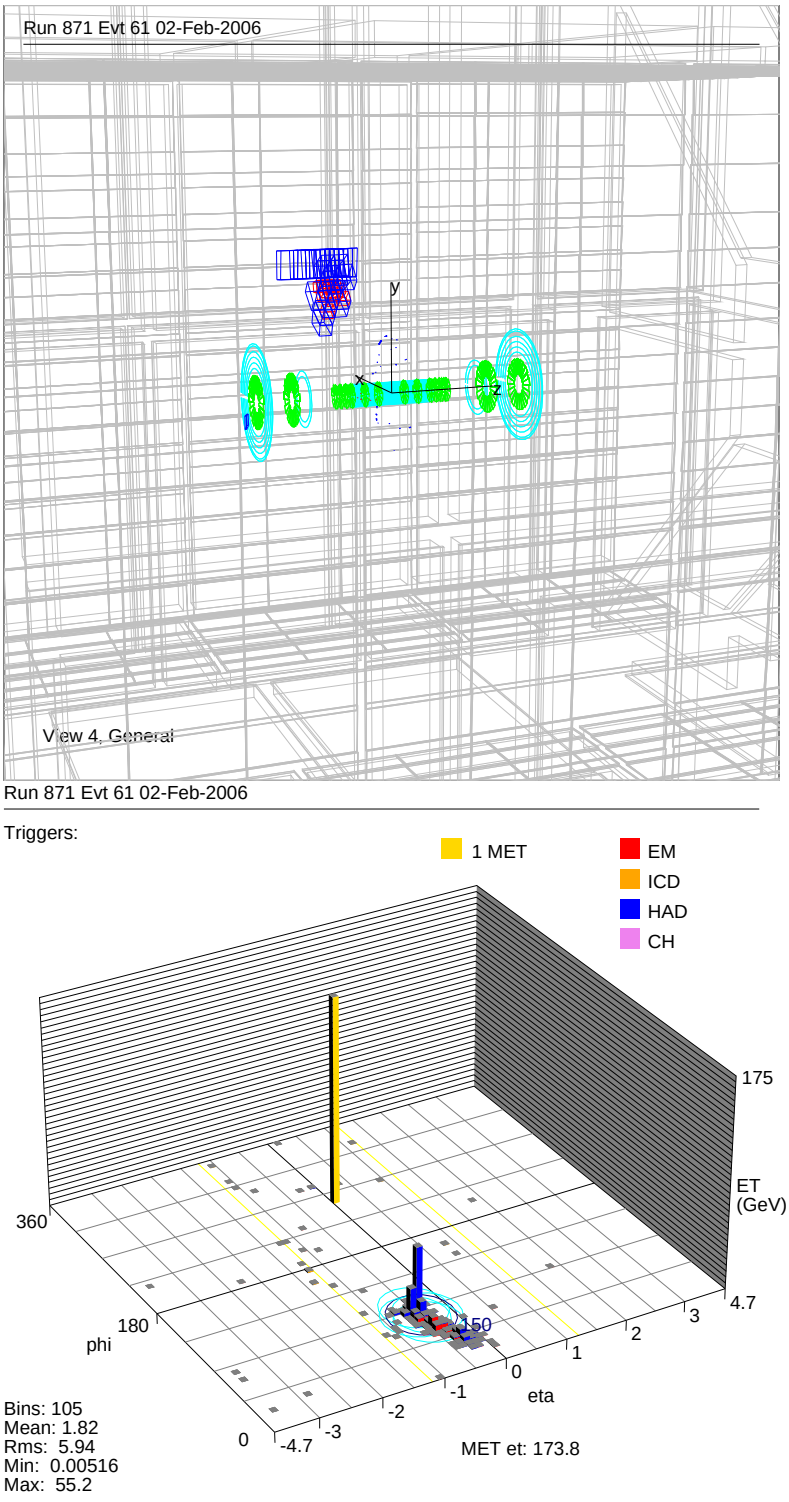

Figure 2: A fairly typical m_G=400 GeV simulated MC event.

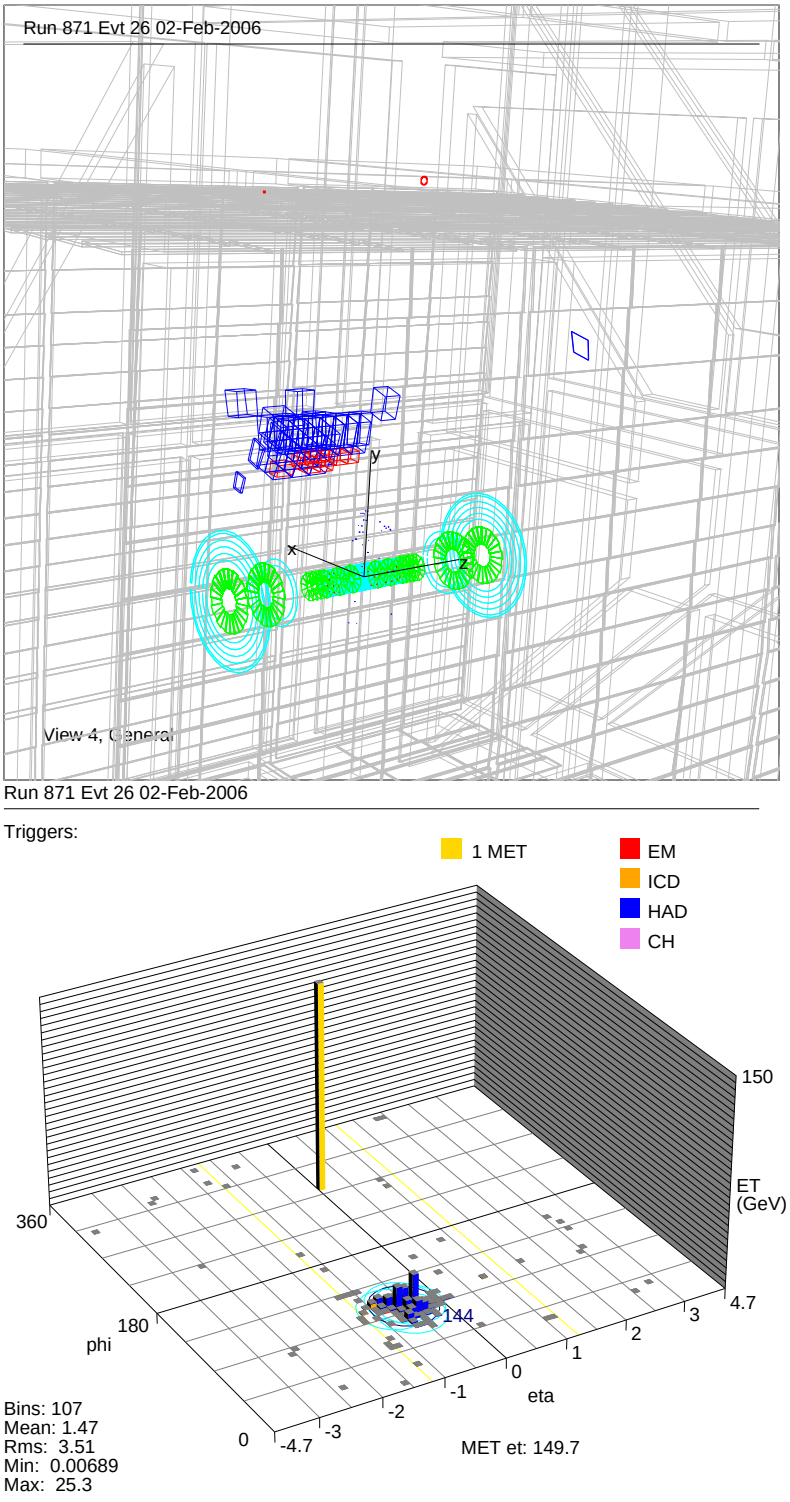

Figure 3: A m_G=400 GeV simulated MC event where the jet was generated nearly parallel to the beam.

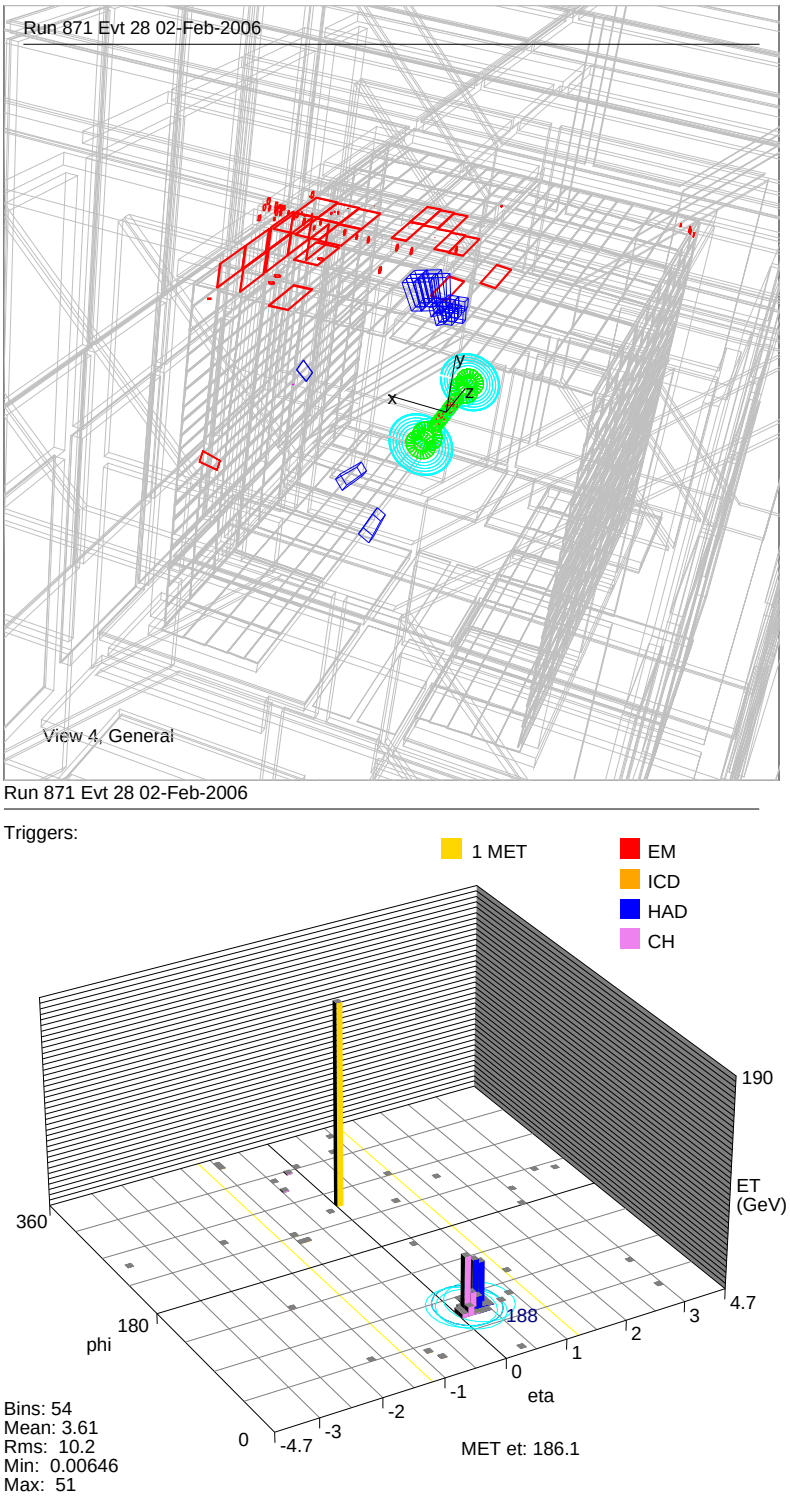

Figure 4: A m_G=400 GeV simulated MC event with a large "A-layer muon splash".

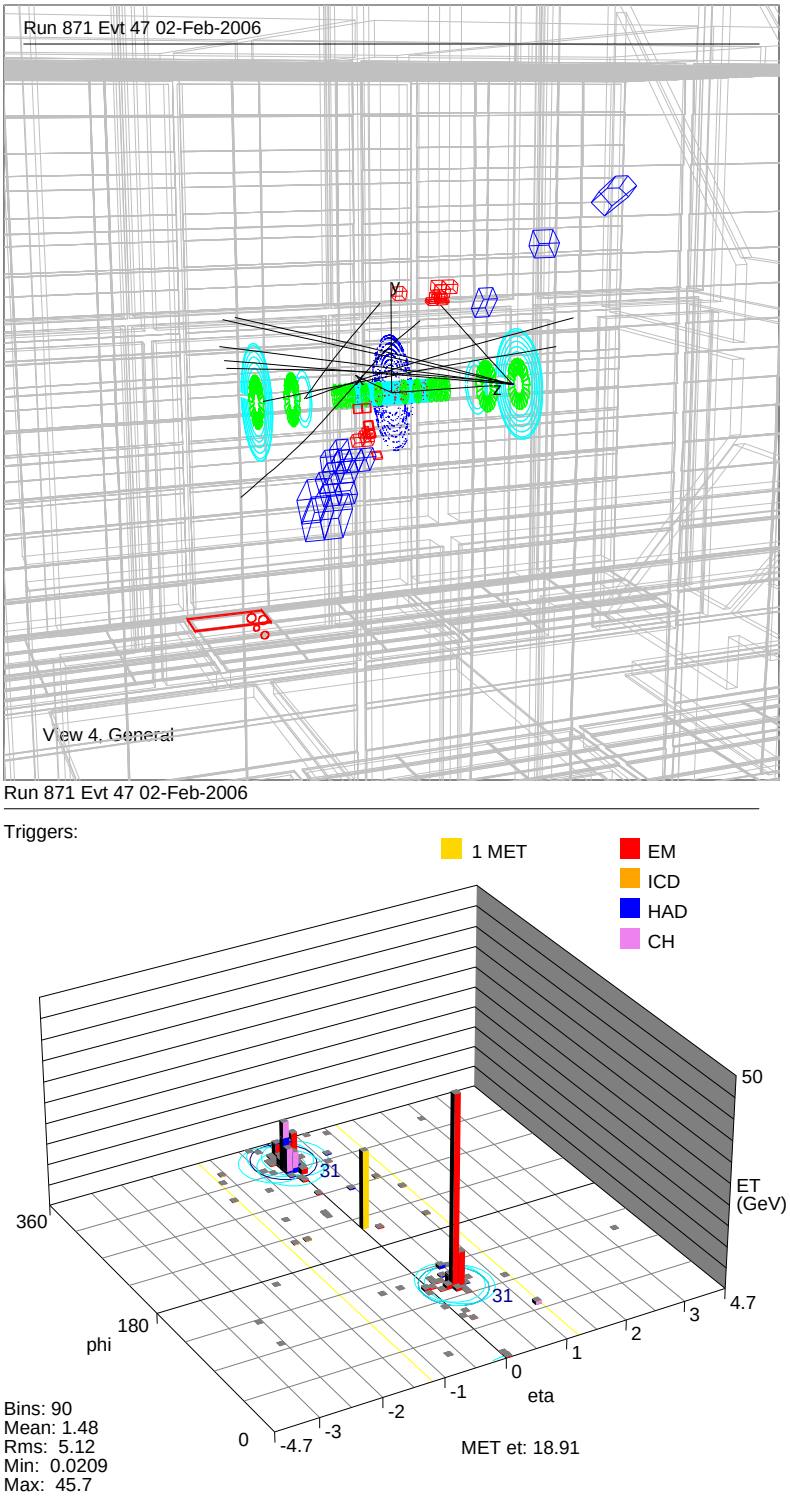

Figure 5: A m_G=400 GeV simulated MC event where some of the shower has gone back across the tracking chamber to the other side of the calorimeter.

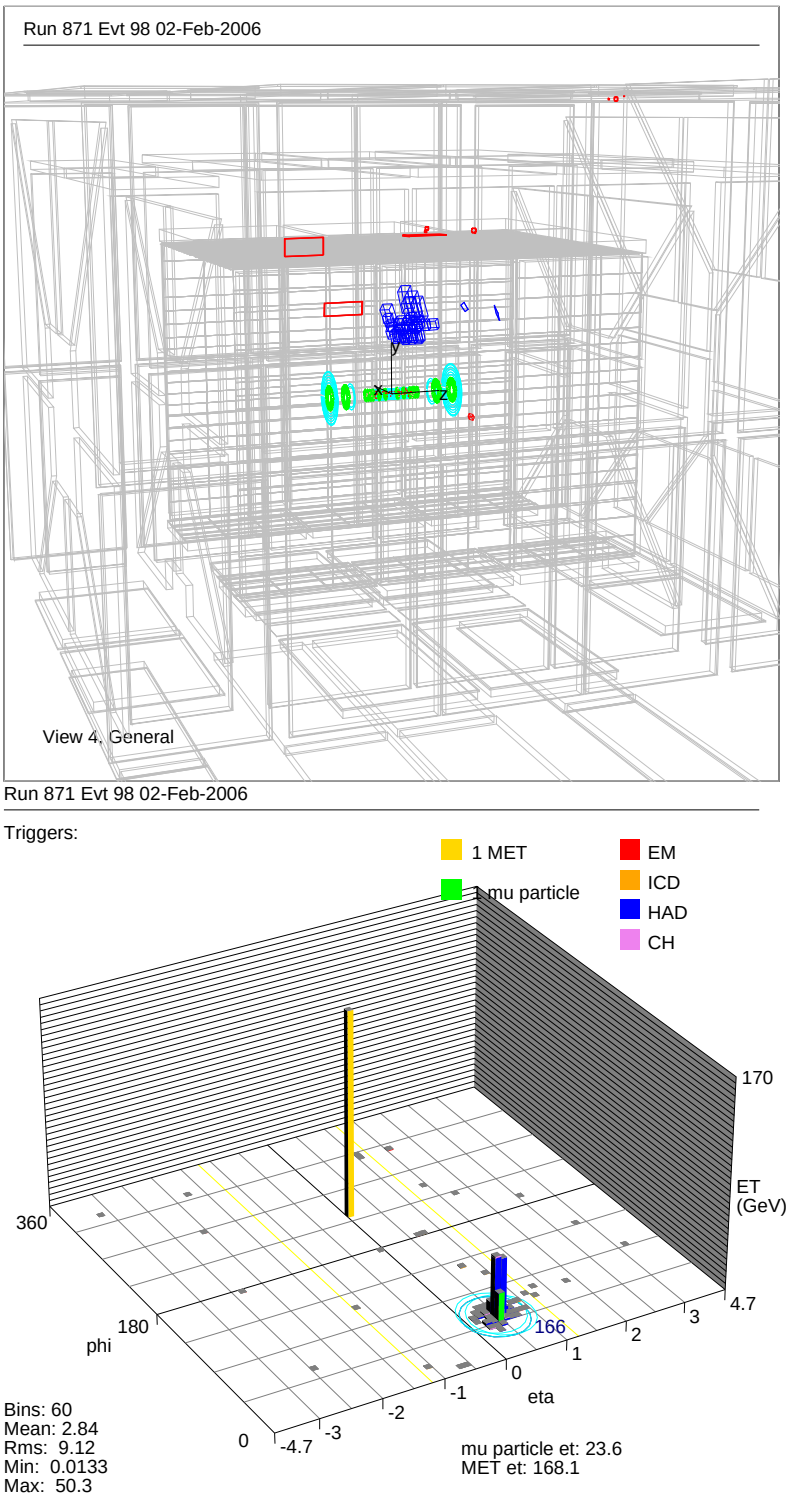

Figure 6: A m_G=400 GeV simulated MC event that has a reconstructed muon from a particle (possibly a muon) punching through the toroid.

5 Pre-selection

In addition to the trigger criteria described above, loose cuts were used to select a initial data sample to study.

- Require "good" muon and SMT and CFT runs, for rejection of cosmic and diffractive events.
- Require exactly one JCCB jet in the event. This helps to reduce certain kinds of detector noise, and also simplifies the analysis.
- Jet E >90 GeV. This avoids noise jets and is also high enough such that the calorimeter part of the trigger is nearly 100% efficient.

6 Sources of Background

We now look at the data to understand the sources of backgrounds that contribute. We will need to understand the backgrounds carefully, in order to be able to devise cuts against them while remaining efficient for signal, as well as being able to estimate the amount of (and energy spectrum of) remaining background as accurately as possible.

The major source of background is cosmic muons. They are able to fake a gluino signal because they can initiate a high-energy shower within the calorimeter. The rate for a cosmic muon to deposit enough energy to pass the basic pre-selection criteria (E>90GeV) is observed to be quite large, about 0.1 Hz. Hard Bremsstrahlung emission is responsible for the majority of the showers. (The probability for a hard-photon of at least 10% of the muon energy to be created in 3m of Iron is about 0.1%.) Fortunately, these showers tend to be very narrow, since they are electro-magnetic in nature and thus have small interaction lengths compared to hadronic showers. Most of the energy is deposited in a few calorimeter cells, see Figure 7. However, sometimes a wide, hadronic-like, shower can be created either due to real deep-inelastic scattering, fluctuations of the shower, or detector effects, as seen Figure 8. Cosmic muons can also mimic other, rarer, signal-like qualities, such as the large muon A-layer "splash", as seen in Figure 9.

Of course, cosmic muons can usually be identified by the presence of a high-energy muon, either entering or exiting the detector, using the muon detectors. In particular, a coincidence of muon hits in the outer two (B,C) layers of the muon system are very strong evidence of a muon. The A-layer hits are often also caused by the signal, due to particles escaping the calorimeters, so these hits are difficult to use for background rejection. (These particles are nearly all absorbed in the Iron toroid magnets before reaching the B,C layers, so do not cause signals often in these outer layers.) In fact, the A-layer hits are used if they are consistent with the geometry of a muon passing through the detector (back-to-back) and not near a hadronic shower. (See section 7 for complete description of these criteria.) However, sometimes no muon is detected, due to detector inefficiencies or the limited detector acceptance up to $|\eta|<2$. Muons can also be detected, in principle, through their ionizing interactions in the calorimeter,

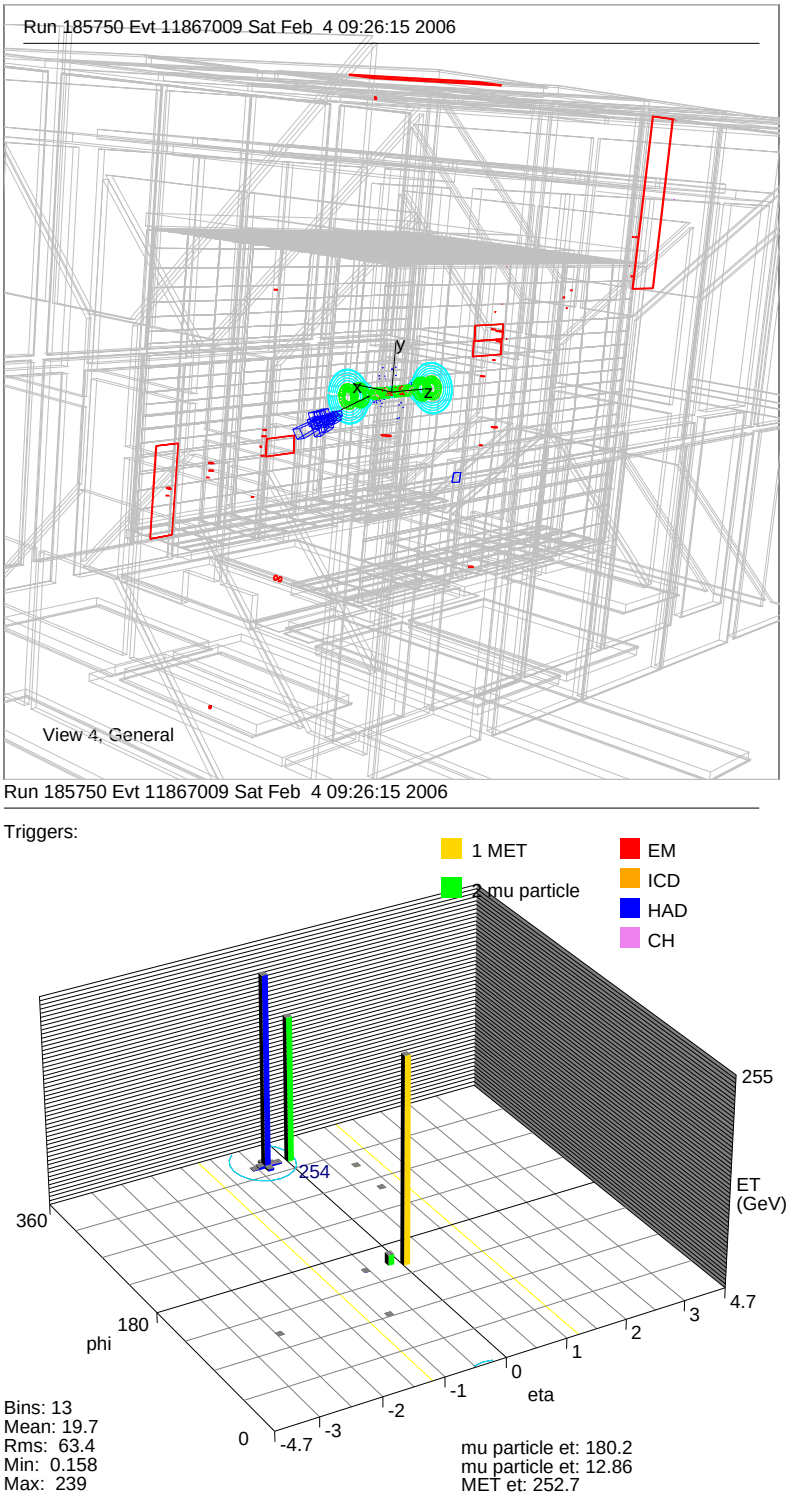

Figure 7: A typical cosmic muon, hard Bremsstrahlung, shower. There are reconstructed muons and a very narrow energy deposit.

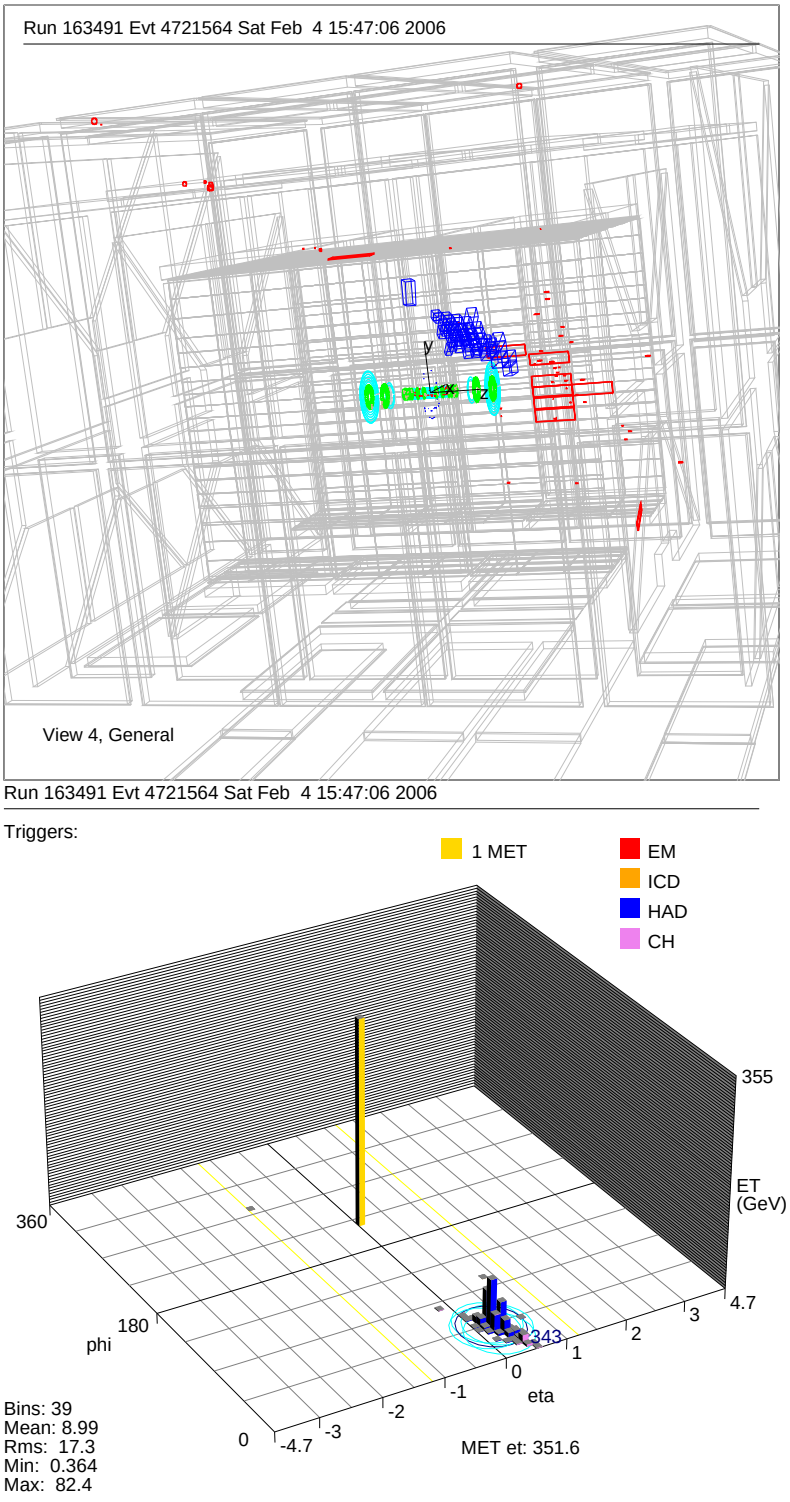

Figure 8: A wide, hadronic-like, cosmic muon shower. This event also contains an A-layer "splash".

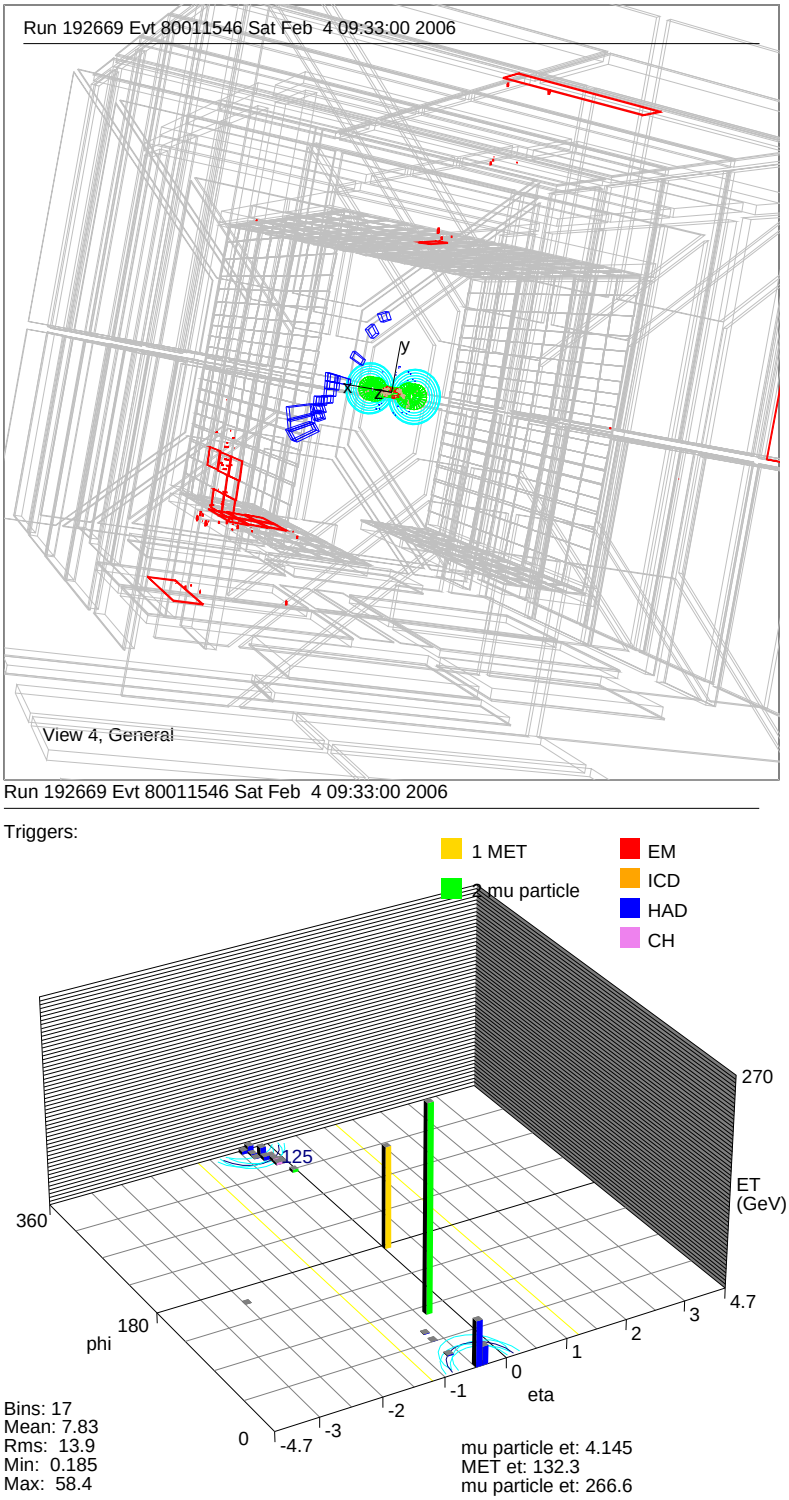

Figure 9: A cosmic muon shower with a large A-layer muon "splash".

where they are minimum-ionizing particles (MIP's). However, these MIP trails are difficult to identify in this geometry where the direction of the muon path is unknown, and also there is a large shower nearby which overlaps with the energy deposited by the MIP. (These MIP tracks are easier to identify for muons on a well-defined path, such as muons traveling outward from $p\overline{p}$ collisions, and when they are not near a jet shower.)

Another source of background events is beam-halo muons, or "beam-muons". These are muons, in-time with the bunches of $p\overline{p}$, and traveling nearly parallel to the beam, as seen in Figure 10. Often, a muon scintillator hit or two can be associated with the muon, and the muon can be seen to be in-time, with Δt<10ns [4]. Another feature of the beam-muons is that they are nearly all in the plane of the accelerator beam, i.e. with ϕ very near to integer multiples of π, as seen in Figure 11. This may be due to the geometry of accelerator magnets or collimators, or gaps in the shielding at either DØ or CDF. Beam-muon showers are also typically very narrow in ϕ-width, even narrower than cosmic muon showers. Since beam-muons are traveling parallel to the beam, the ϕ-width is small no matter how long the shower extends along the path of the muon. For the same reason, the η-width of beam-muons tends to be larger than for cosmic muons. Comparisons of these quantities for beam-muons and cosmic-muons can be seen in Figure 12.

Since we are using the GAPSN triggers, nearly all of the $p\overline{p}$ beam produced backgrounds are eliminated. An exception is double diffractive events with large momentum transfer. Figure 13 shows and example of such an event. However, after requiring no PV to be reconstructed and large $\not\!\!E_T$ (implicit from the choice of only one central jet with E>90 GeV), these events are eliminated. Di-jet events in the same data sample were studied to understand the $\not\!\!E_T$ spectrum and PV reconstruction efficiency for beam-related backgrounds.

Other small sources of background considered are cosmic neutrons and neutrinos. Neutrons would be more effective in creating wide hadronic showers, but their rate is about 1/1000th that of cosmic muons of similar energy, and they also would be unlikely to penetrate the Iron toroid magnets. In the event that one did reach the calorimeter, they would most likely shower in the outer coarse-hadronic layer, which is not part of the L1 calorimeter trigger. Thus, we expect that the number of cosmic neutron events in the data sample is very low. Neutrinos are copious, but have a very low interaction rate. A back-of-the-envelope calculation predicts a neutrino-shower rate of about 0.1/year.

Finally, since we are looking for a very rare process, occasional detector malfunctions could also fake a signal. However, these problems tend to be isolated to a specific set of runs, a specific detector region, or both. See Figures 14 and 15 for displays of the most frequent problems. Also, the detector problems would have to be correlated between the calorimeter and muon systems in order to pose a significant background in this analysis while not being detected in other control samples.

[4] Δt for muon hit is (time hit occurred) - (time a hit would occur from a muon coming from the beamline in this bunch crossing). So, it's the extent to which the hit is early or late, compared to a hit from a "standard muon", traveling at speed c from the beamline.

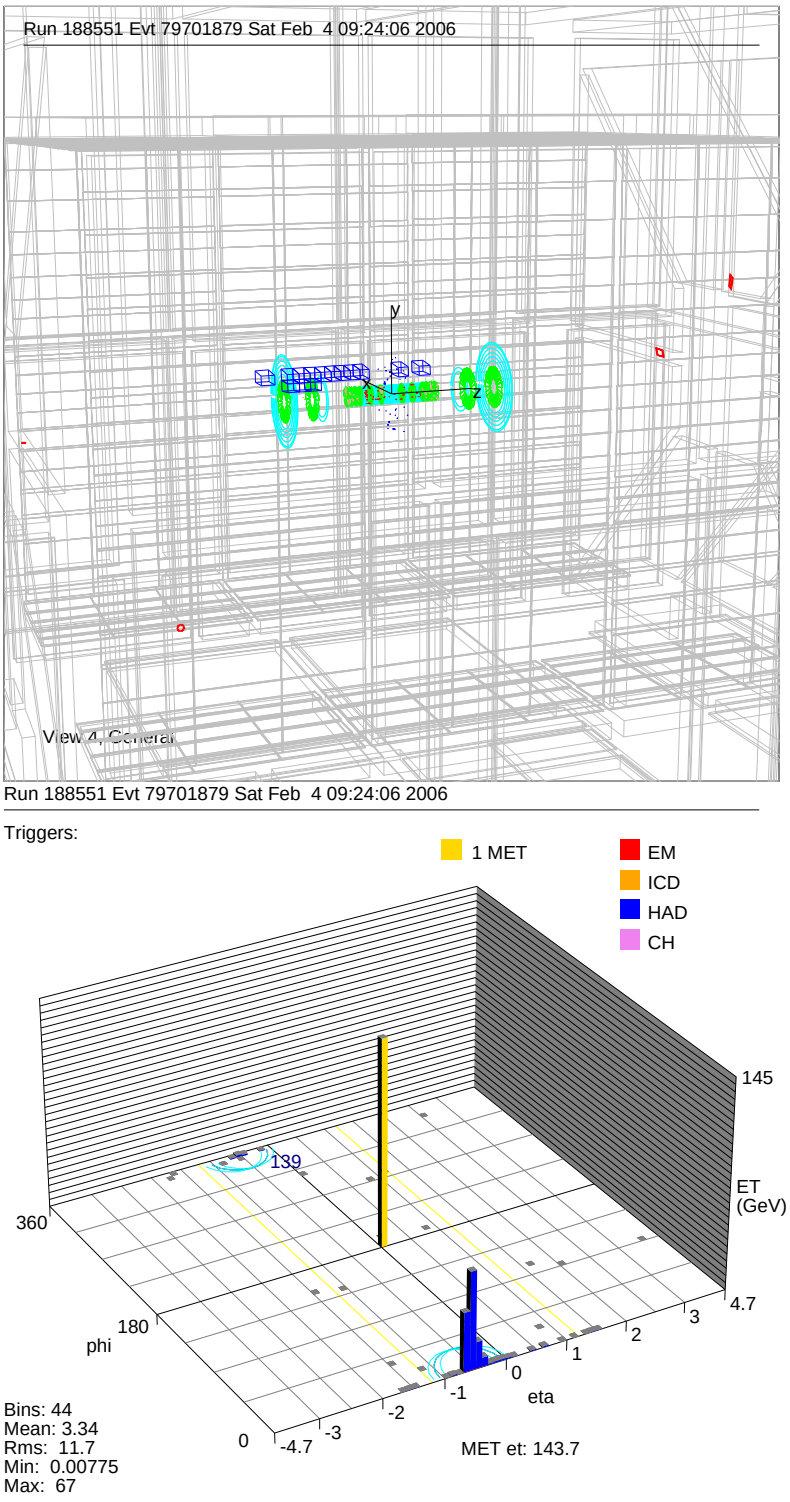

Figure 10: A typical beam-muon shower. The jet is very narrow in ϕ, but long in η, and centered at an integer multiple of π (in the plane of the accelerator).

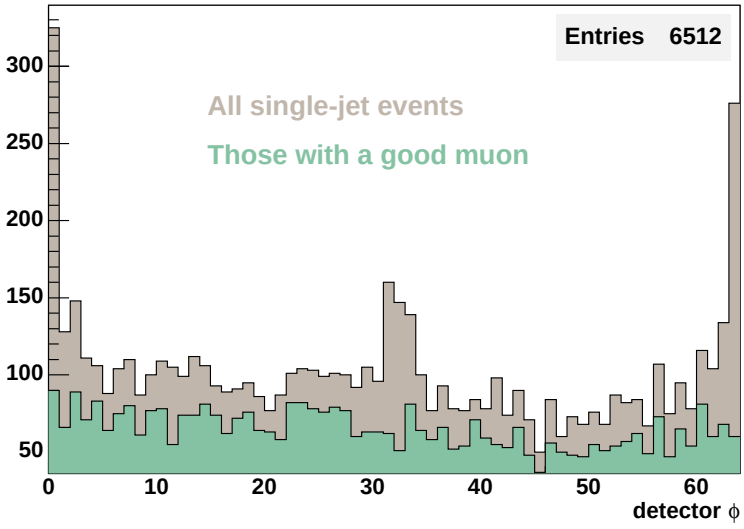

Figure 11: The ϕ of jet showers from all sources, beam-muons and cosmic-muons (grey), and good cosmic muons (green). The beam-muon showers are highly localized near integer values of π, in the plane of the beam.

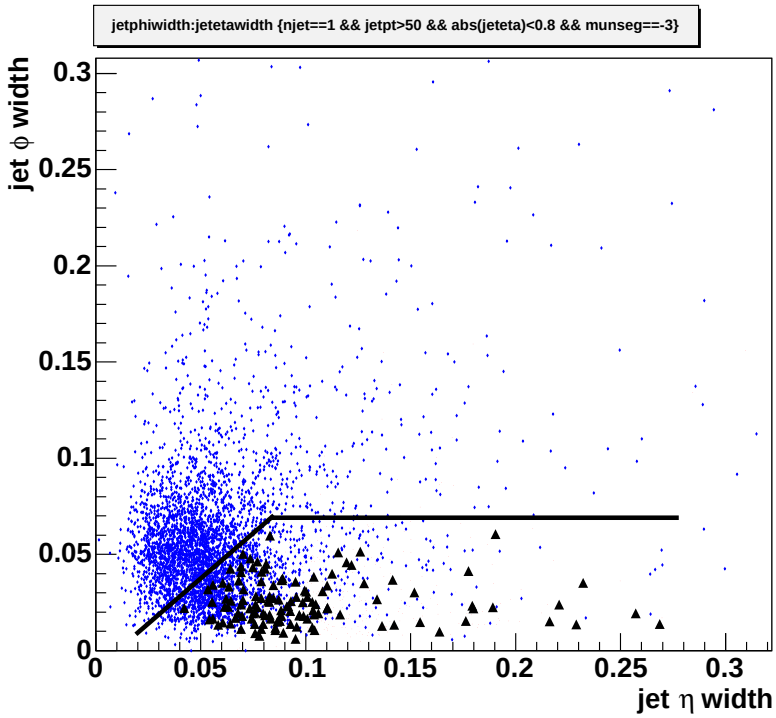

Figure 12: The ϕ vs. η of jet showers from beam-muons (black triangles) and cosmic-muons (blue dots). The beam-muon showers are selected by requiring an associate "in-time" muon scintillator hit. The beam-muons are narrower in ϕ-width but wider in η-width than the cosmic showers, due to the fact that they are parallel to the beam.

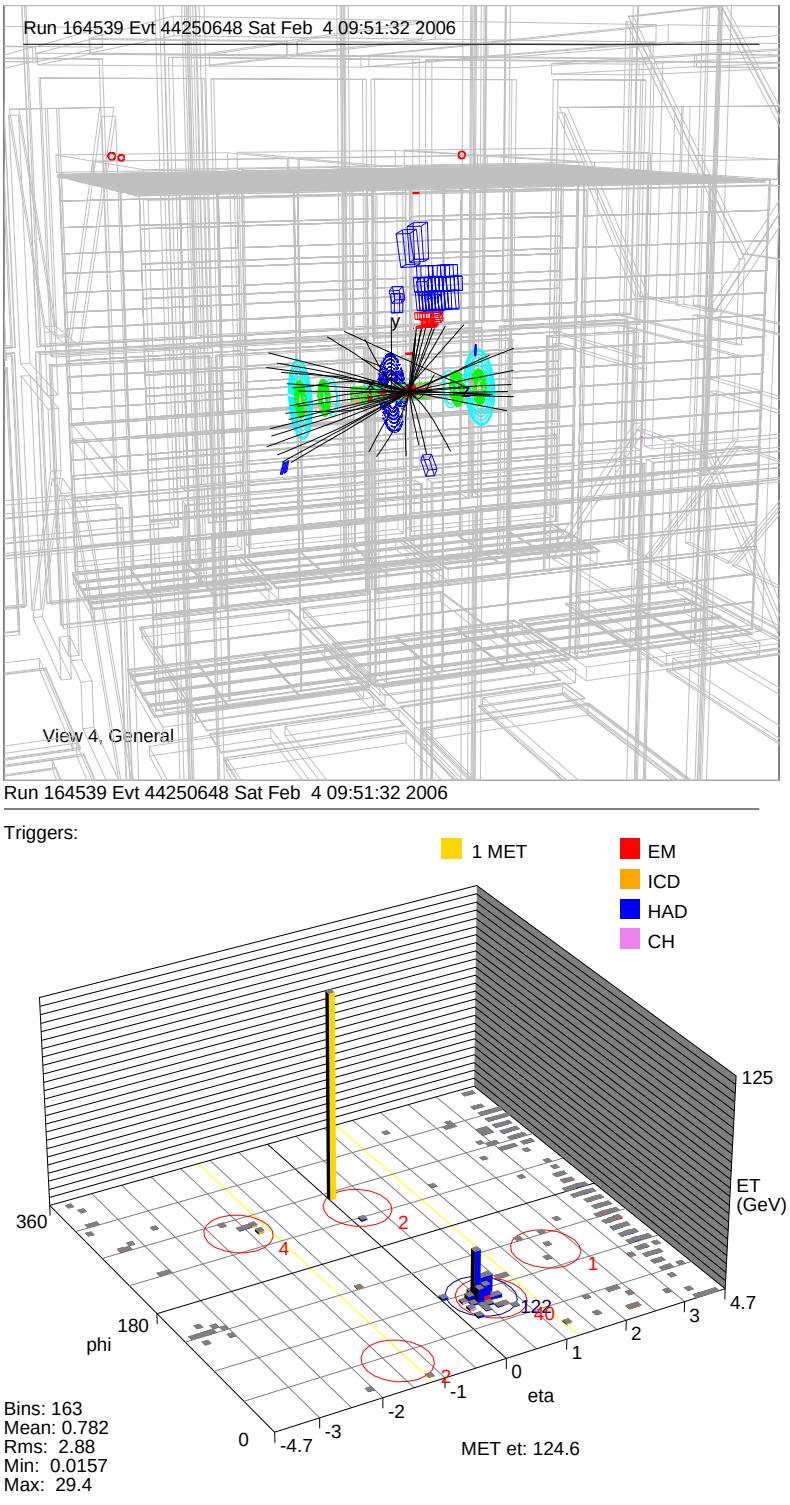

Figure 13: A typical diffractive event with a single observed jet.

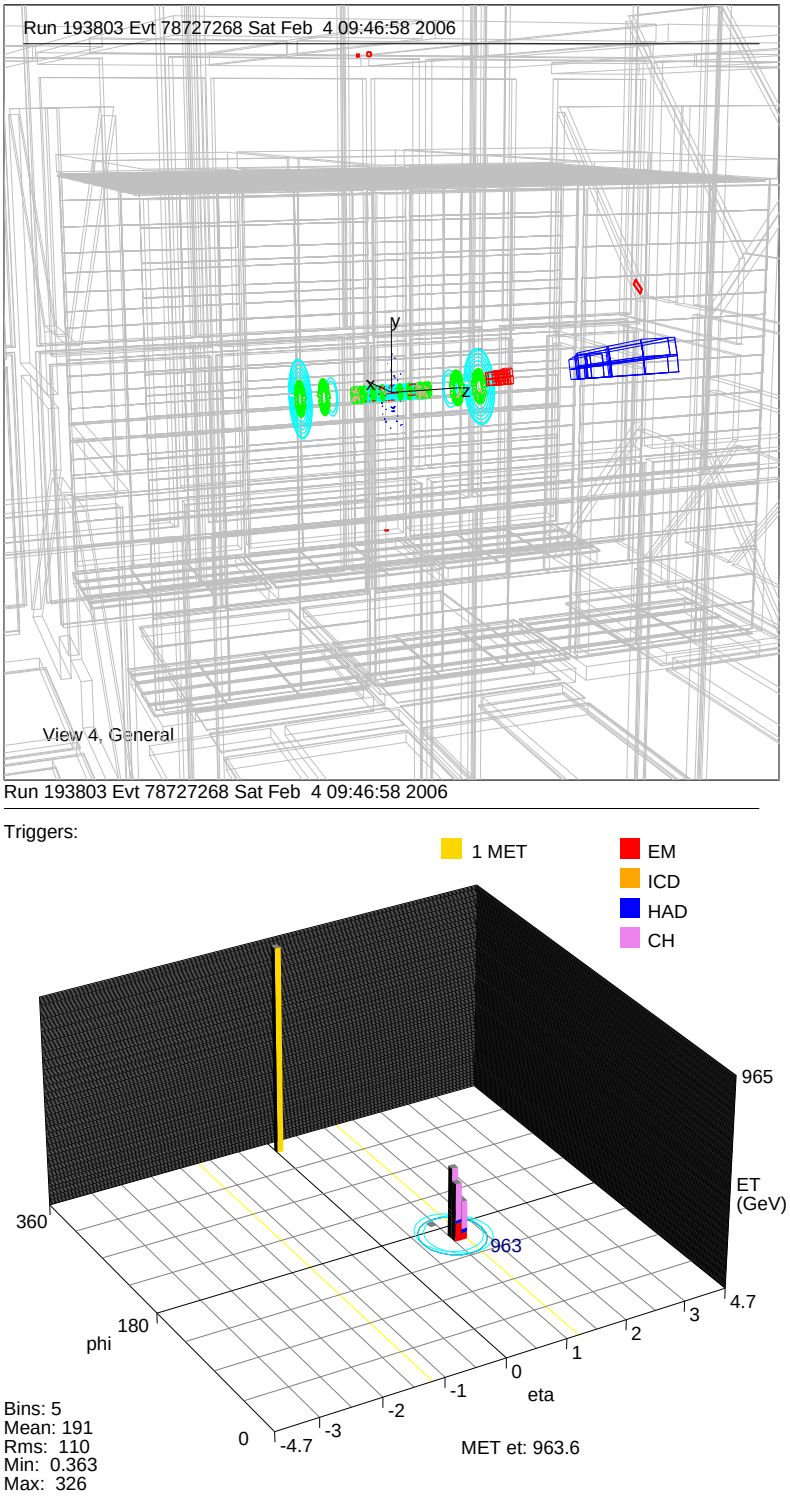

Figure 14: A detector problem event with a jet in a typical hot-spot. This hot region appears only in one run of the data set, and is also beyond the η<0.9 region used for analysis.

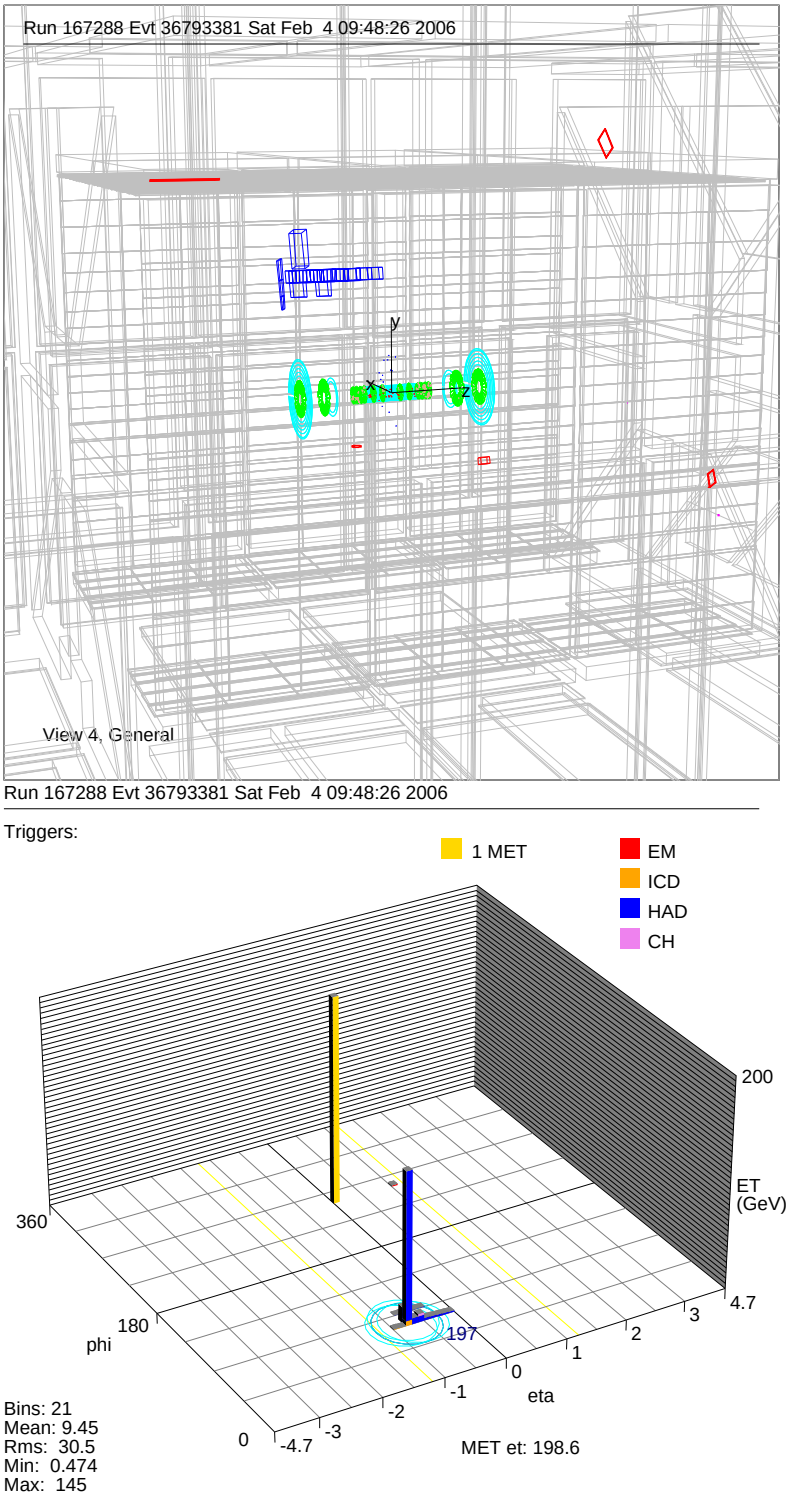

Figure 15: A detector problem event with a jet in a typical hot-spot. This hot region appears in many runs throughout the data set, and so is removed.

7 Event Selection

Now that the background sources are understood and the gluino signal is simulated, we can make selections to reduce the backgrounds while still remaining efficient for the gluino signal.

- Jet $|\eta|$<0.9. The ICR and forward regions of the calorimeter were observed to have some difficult detector problems (hot spots). Also, the gluino signal tends to be concentrated in the central regions.
- No reconstructed primary vertex. This usually means that no tracks were reconstructed, although sometimes a track was found but does not come close to the beam axis. This requirement removes background from diffractive events very effectively.
- The rectangular region ($-.55 < \eta < -.75$, $1.3 < \phi < 1.5$) was too noisy and therefore all events in that region were rejected. (See Figure 15 above.)
- Jet E <900 GeV. This avoids certain kinds of detector problems and is besides un-physical for a gluino at the Tevatron.
- Jet ϕ-width and η-width were both required to be <0.25 to eliminate events from certain types of detector problems, such as when pulsers were accidentally activated.

Further selections are then applied. The following criteria are used to select events containing "wide showers". (All jets which fail these cuts are considered "narrow showers" or "narrow jets".)

- Jet η-width and ϕ-width >0.08.
- Jet n90 >=10. This prevents fake wide showers from a narrow muon shower plus a long MIP trail.

These following criteria are used to select events containing "no-muon". (Events failing these criteria are considered "muon-jets" or "muon-events".)

- No $|NSEG| = 2$ or $|NSEG| = 3$ muons in the event. These events are nearly all cosmic muons (although we do lose about 10% efficiency here for gluino events).
- Require the $\Delta\phi$ between all pairs of A-layer ($|NSEG| = 1$) muons to be <1.5. Gluino jets often leak into the A-layer a bit, but we want to veto on back-to-back A-layer muons that could come from a single cosmic muon.
- Require the $\Delta\phi$ between any A-layer ($|NSEG| = 1|$) muon and the jet to be <1.5. We want to allow the jet to leak into the A-layer, but veto events where the A-layer muon is not associated with the jet (since it is then likely to be due to a cosmic muon).

A candidate gluino shower would be both wide and contain no muon, a so-called "wide no-muon shower". Figures 16 - 18 show displays of some of these candidate events. Figure 19 shows histograms of the properties of the candidates events.

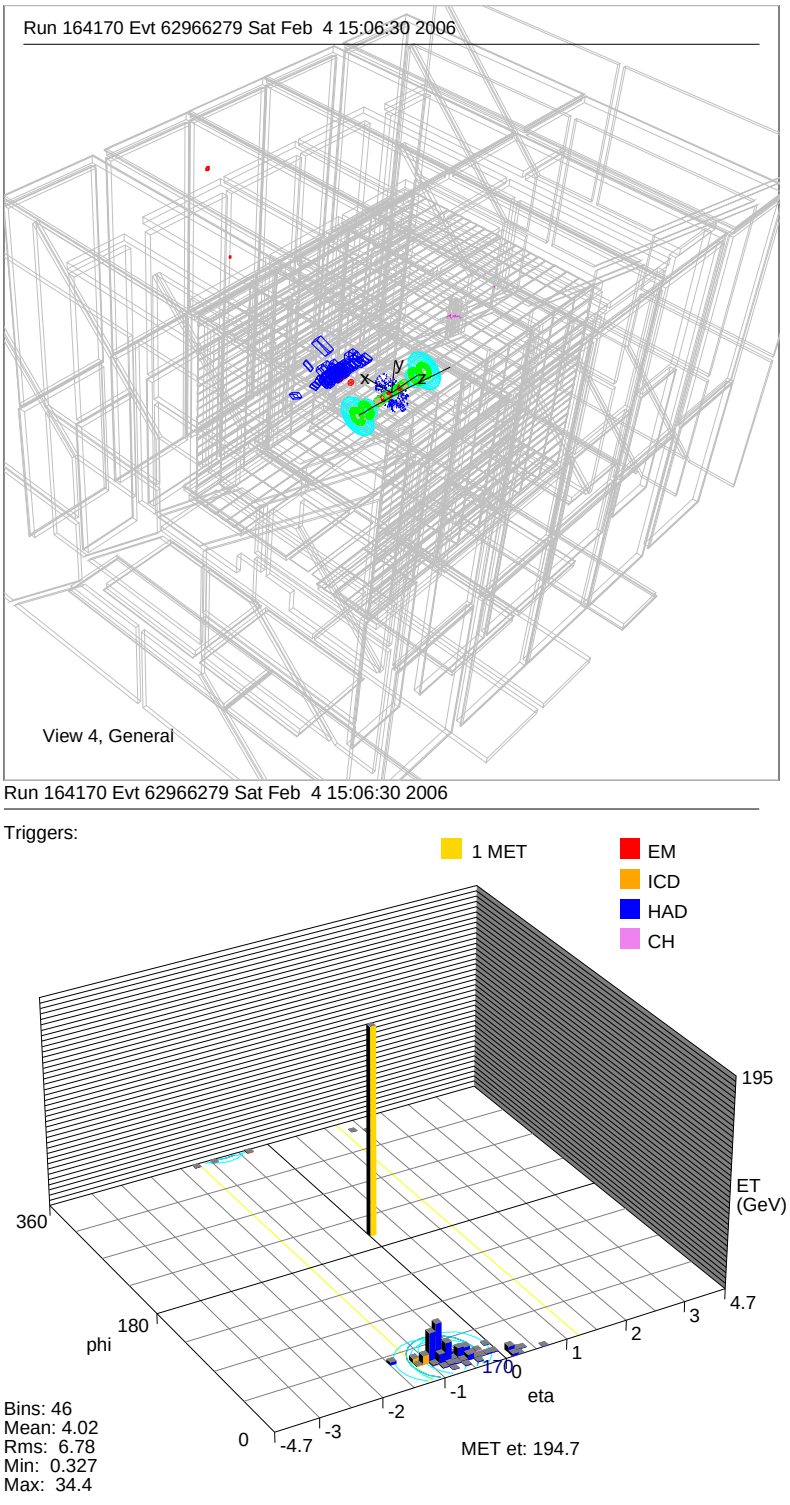

Figure 16: A typical candidate signal event, a wide shower, with no good muon.

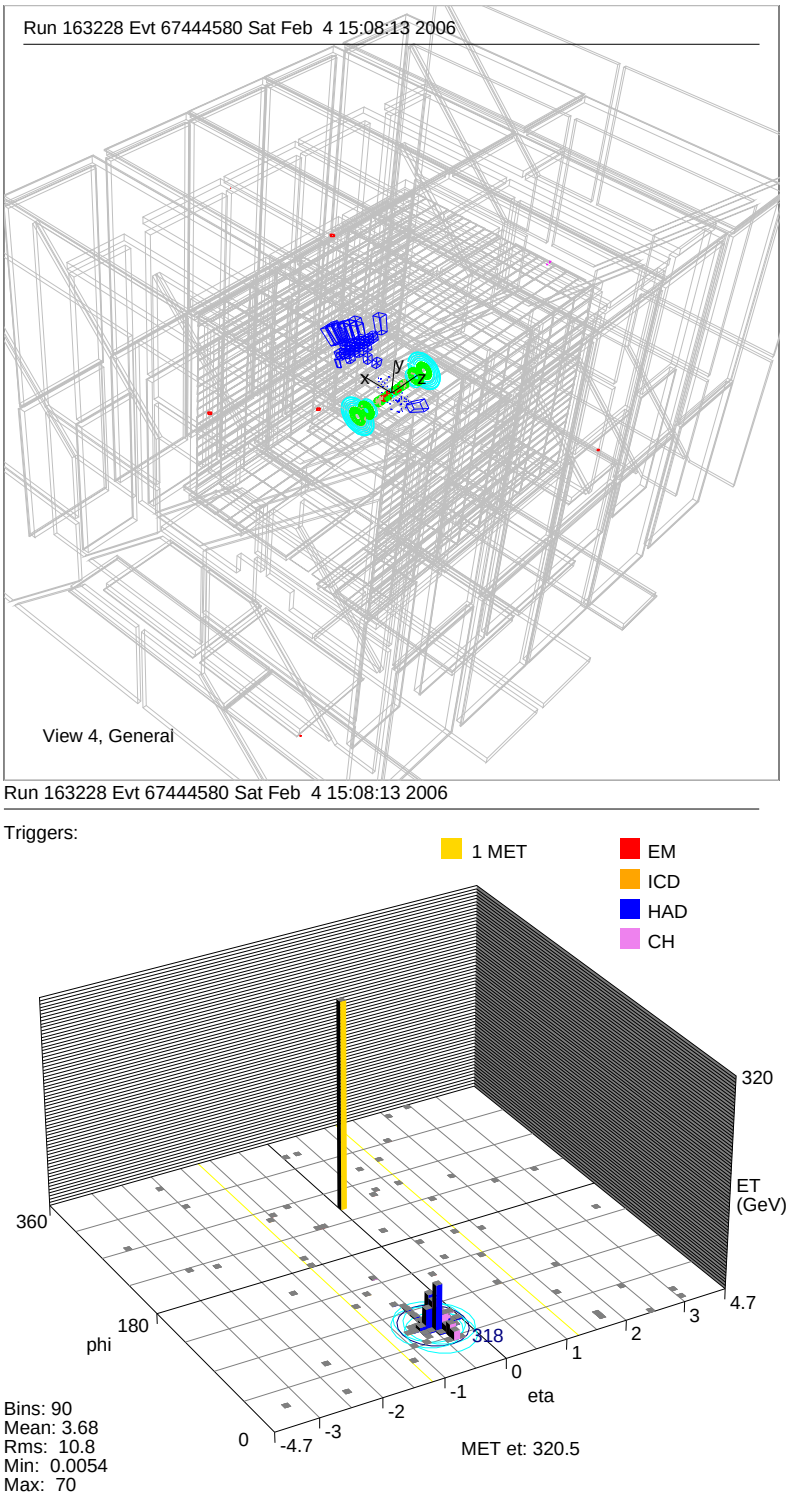

Figure 17: A typical candidate signal event, a wide shower, with no good muon.

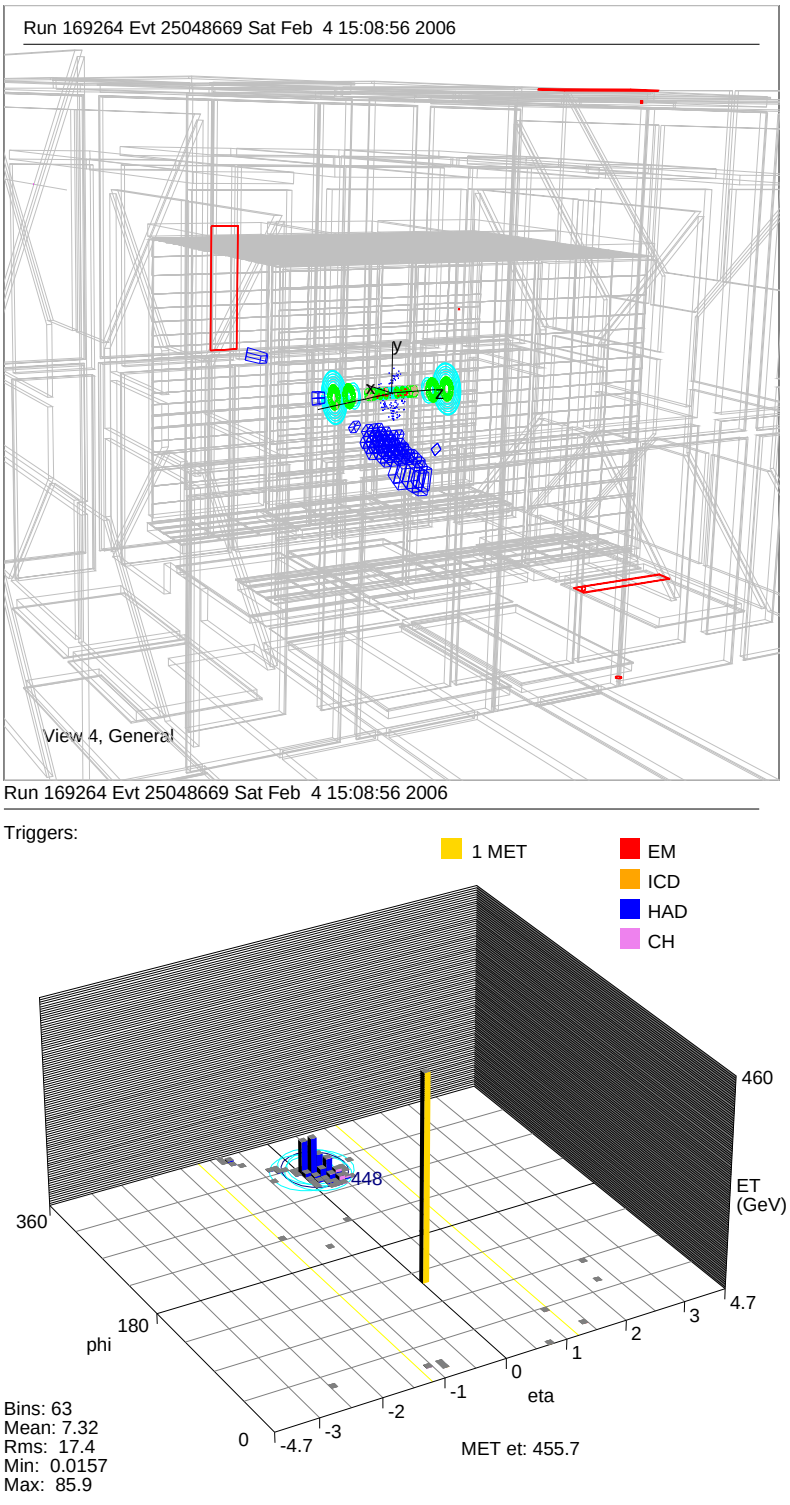

Figure 18: A typical candidate signal event, a wide shower, with no good muon.

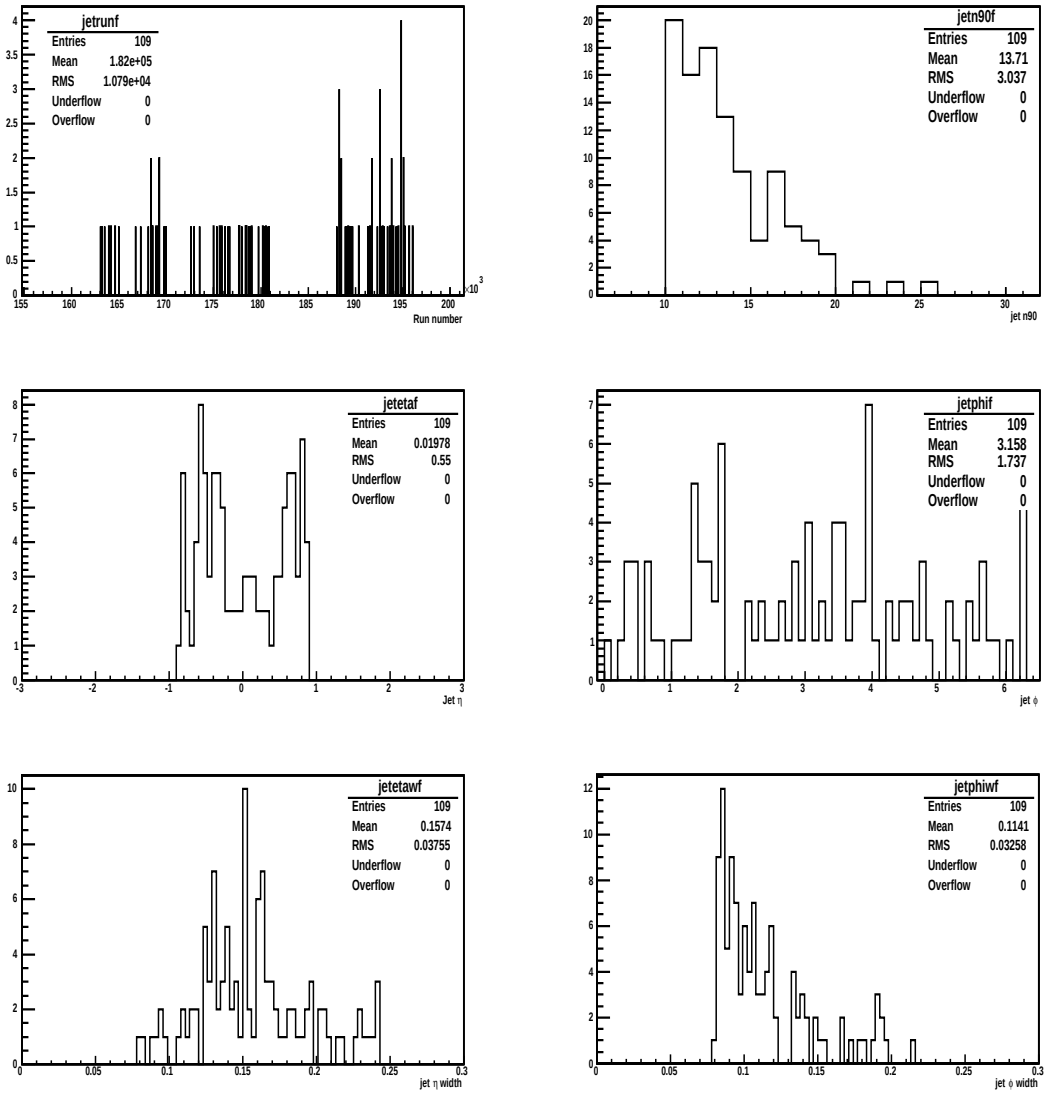

Figure 19: The properties of the candidate events, those with a wide-jet shower and no-muon. From left to right and top to bottom, the run number of the event, the jet n90, η, ϕ, η-width, and ϕ-width.

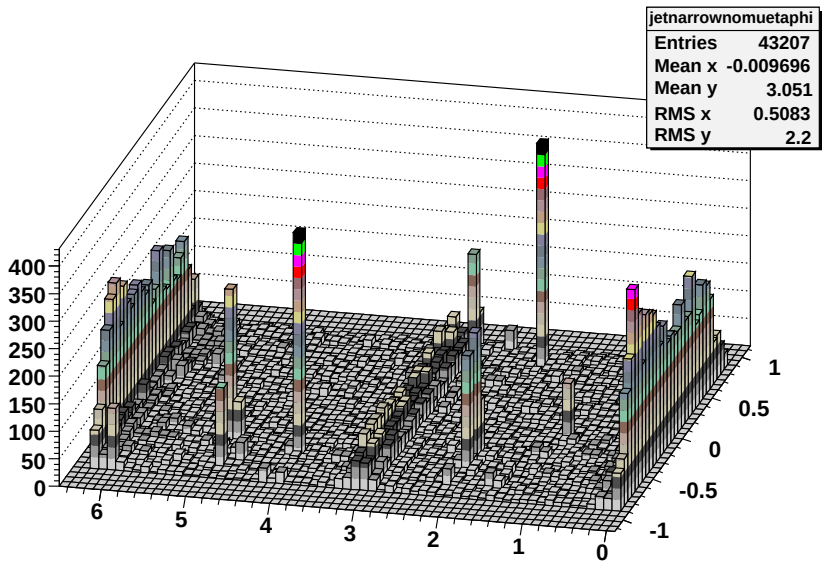

Figure 20: A histogram of the narrow-jet η vs. ϕ, showing the hot spots present for the narrow-jets, as well as the ridges from beam-muons.

8 Background Determination

To estimate the number of wide no-muon showers to expect from background (cosmic muon showers that happen to be wide and in which we happen to not see the muon), we use the assumption that the probability to not reconstruct the cosmic muon is independent of whether the muon shower is narrow or wide. Thus, we first measure the probability to miss the muon (P_{nomu}) in the narrow-jet cosmic data sample. Then this probability is applied to the wide-jet cosmic-muon data sample to predict the number (and energy spectrum) of wide-shower no-muon background events.

However, there are two complications that must first be dealt with in the narrow-jet sample before we can measure P_{nomu}. First, there are hot spots (detector problems / noise) that occur in the narrow-jet sample that are not manifested in the wide-jet data. This is understandable, since many detector problems and noise can be isolated to a single calorimeter cell or a small group of cells, and thus would lead only to narrow fake jets. These hot spots are removed from the narrow-jet sample before P_{nomu} is measured, using the following procedure. A 2-dimensional histogram is made of the narrow-jet phi vs. eta, as shown in Figure 20. We can see that there are at least 5 regions that are very "hot". And we also observe the pattern of beam-muons that exist near integer multiples of ϕ/π (in the plane of the beam). Since we wish to remove both these sources of narrow-jets (further methods are discussed below to deal with the remaining beam-muon-induced narrow-jets), hot regions of this histogram will be excluded. Any bin with more than 50 entries is considered a "bad" region, and is excluded when measuring P_{nomu}. The resulting phi vs. eta distribution after this cut is shown in Figure 21.

The second issue to be dealt with in the narrow-jet sample, as already alluded to, is that there is contamination from beam-muons. The beam-muon events have different

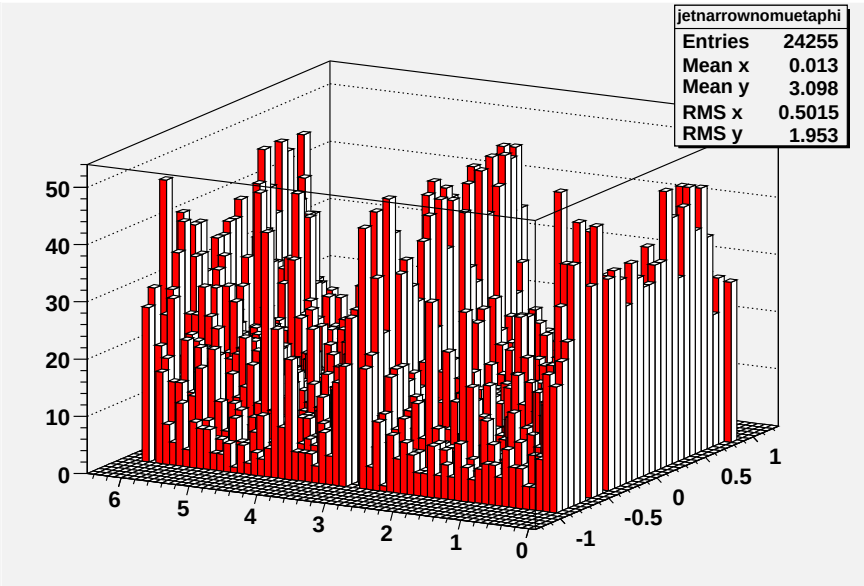

Figure 21: A histogram of the narrow-jet η vs. ϕ after cutting at 50 entries, showing that the hot spots present for the narrow-jets have been removed. Some of the ridges from beam-muons remain.

properties than the cosmic showers, due to their production mechanism and the angle that they tend to enter the detector from. Their energy spectrum is different from the cosmic showers, and falls off faster with energy (for instance, there are no showers above 1 TeV!). Because they enter parallel to the beam-line, they can not readily induce showers with large ϕ-width, so they do not contribute significantly to the wide-jet events. And since they preferentially enter the detector near the far-forward region where muon acceptance is smaller, it is more likely to not reconstruct the muon in beam-muon events. For all of these reasons, it is critical to remove the contribution from beam-muons when measuring P_{nomu}.

We can use the fact that the energy spectrum is softer for beam-muon events in order to separate them from cosmic-muon events. If we plot P_{nomu} as a function of jet energy, as in Figure 22, we see that P_{nomu} decreases vs. energy to a plateau of about 10%. The hypothesis is that beam-muons cause P_{nomu} to be larger at low energy, and evidence for this will now be shown. We can fortunately study the properties of nearly-pure beam-muon showers whenever we do reconstruct the muon, since this muon is in-time ($|\Delta t|$<10ns) and the shower is near the plane of the beam, as shown in Figure 23. If we plot the fraction of in-time muons vs. energy, as in Figure 24, we see that the fraction decreases steadily vs. energy towards a plateau of about 5%. If the muons were all of cosmic origin, and thus flatly distributed in time, the fraction of muons that randomly happened to be in-time would be 20ns / 396ns = 5%. (The $|\Delta t|$<10ns criteria implies a time window for in-time muons a total of 20ns wide.) Thus, at high energy (above 400 GeV), there is a negligible contribution from beam-muons. So we can measure P_{nomu} in the region above 400 GeV, as was shown in Figure 22, and arrive at P_{nomu}=0.11$\pm$0.01.

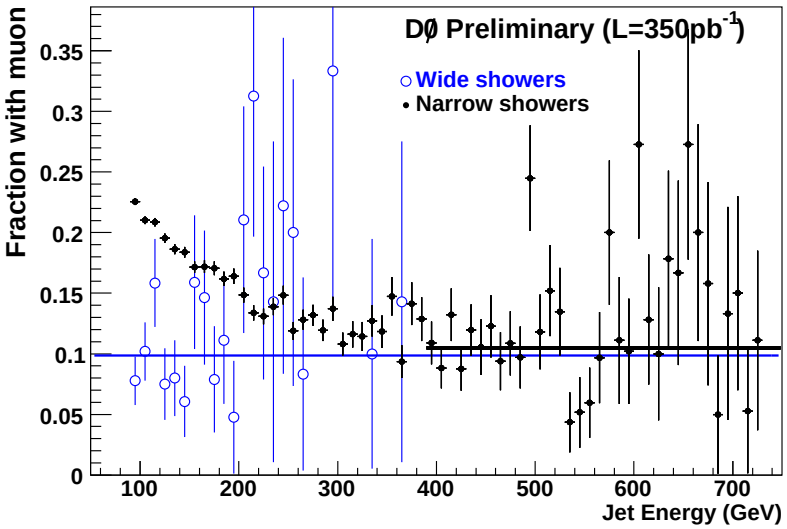

Figure 22: The ratio of the number of wide (blue circles) and narrow showers (black dots) with muons to the number without muons, vs. jet shower energy. Also shown are the fits (to constants) to both distributions.

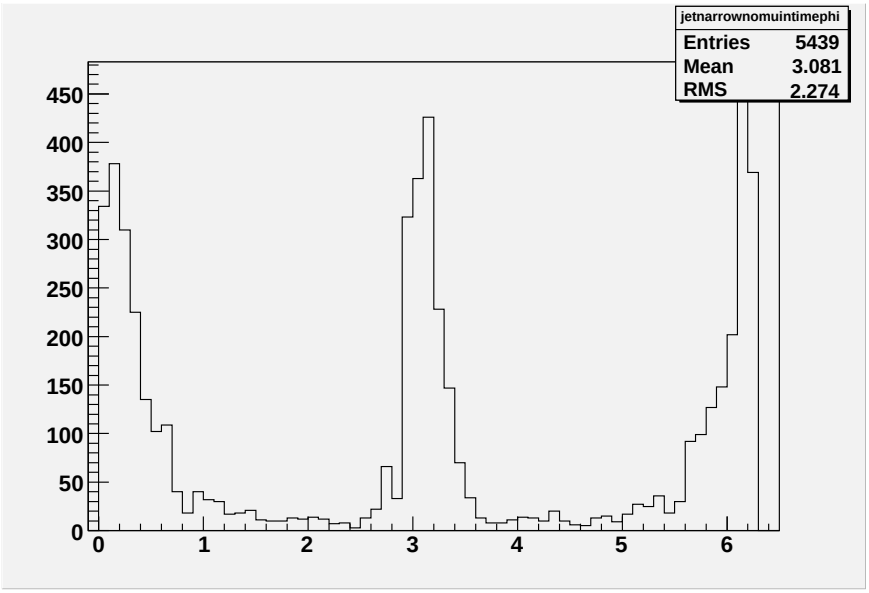

Figure 23: The ϕ distribution of in-time A-layer muons in narrow-jet showers.

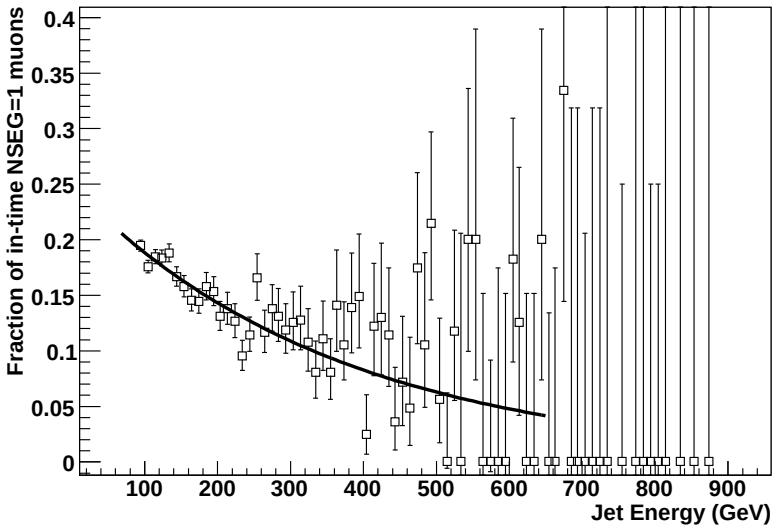

Figure 24: The fraction of in-time A-layer muons in narrow-jet showers, vs. jet shower energy.

Sample	1 Jet	$\|\eta\|$	E>90	No PV	W.<.25	W.>.08	n90	No mu
200	0.91	0.91	0.30	0.98	1.00	0.57	0.85	1.00
300	0.87	0.89	0.97	0.97	1.00	0.50	0.86	0.96
400	0.83	0.89	0.99	0.96	0.99	0.56	0.89	0.97
500	0.81	0.91	0.99	0.97	0.99	0.56	0.85	0.97

Table 1: The signal efficiencies for each cut, for each simulated gluino mass sample.

9 Signal Efficiency

To first order, the detection efficiency for the stopped gluino signal events can be estimated from the MC simulation. The fraction of events falling outside the jet energy cuts, $|\eta|$ cut, n90 cut, and jet η-width and ϕ-width cuts can be fairly accurately predicted. Table 1 shows the efficiency for each criteria.

Some effects are not modeled in the MC, however. Table 2 shows the additional sources of inefficiency and the total efficiency to be multiplied by the MC acceptance. The final signal efficiencies are shown in Table 4.

For instance, there is a loss of efficiency at the trigger level from the GAPSN requirement. If a min-bias event happens to occur during the bunch crossing when the gluino decays, the GAPSN trigger will not fire. The fraction of the time this occurs has been measured using cosmic-muon shower events [5] triggered on the JT_125TT trigger from the "QCD" skim. It is observed that 75% of the time that JT_125TT fired, the

[5]These are mostly narrow-jet showers, but no explicit requirement on the shower was made. The cosmic muon requirement means that the muon had timing information, and it was "out-of-time" with the bunches. This is rejection against beam-muons.

Source	Efficiency
GAPSN Trigger	.6
Trigger gaps	.68
Total	0.41

Table 2: The extra signal inefficiencies, and their total product.

JT_45TT_GAPSN trigger also fired, thus the efficiency of the GAPSN trigger term, for cosmic-muon showers, averaged over the PASS2 data set, is 75%. The probability to have no min-bias interactions during a given crossing is proportional to $e^{-\lambda}$, where λ is the average number of interactions per crossing, which is proportional to the instantaneous luminosity. For this data set, $\lambda \simeq 0.3$. However, since it is more likely that the gluino decay occurs during a time close to its production (compared to the length of a store), the inefficiency is actually a bit higher. Since the gluino lifetime is unknown (but presumed to be less than a few hours), the inefficiency is unknown, but we will conservatively estimate it to be 60±15%. In a worst case, if all the gluino decays occurred when the luminosity was twice that observed on average, the efficiency would be $.7^2$=50%. In the best case, the efficiency would not depend strongly on the instantaneous luminosity.

Another source of inefficiency is that the trigger is not live all the time, but only during the "live super-bunches", see Figure 25. During the sync-gap and each of the two cosmic-gaps, the triggers are dead[6]. The live super-bunches make up 68% of the total accelerator turn time, with minimal uncertainty.

Finally, there is also a shift of the observed jet energy towards lower energies whenever the calorimeter signal from the gluino decay is not in-time with the bunch-crossing time. This is due to the fact that the calorimeter electronics samples the shaped calorimeter signal only once, at the assumed peak of the signal, assuming that the signal is a maximum near the start of the bunch crossing (when ions begin to drift), see Figure 26. The amount of inefficiency can be measured by looking at cosmic-muon showers where the muon has been reconstructed. Very little falloff in efficiency can be seen vs. the muon time, as seen in Figure 27, as expected since the time window (up to only 50ns [7]) is short compared to where efficiency should start to drop (around 140ns). So we need to measure the efficiency for muon showers outside this time window. The muons in the time window from 10-50ns are free from beam-muons (nearly all of which are in-time: Δt<10ns) and have their times well measured. The number of muons in this time range is 2983 (in a subset of the full data). The number of muon showers outside this range (in the same data subset) and also not in-time, is 17254. The inefficiency is thus: (17254/2983)/((396ns-40ns-20ns)/40ns) = 5.8/8.4 = 69%. This same inefficiency can be created if the average shower energy is decreased by 15%, causing some events to fall below the jet energy threshold. Instead of assigning an efficiency

[6]A trigger which fires during the cosmic gaps (21% of the turn) is under discussion for future use. It is not possible for DØ to trigger during the sync gap (11% of the turn), when crate electronics are performing other tasks.

[7]The muon scintillator time window is limited by the muon readout electronics.

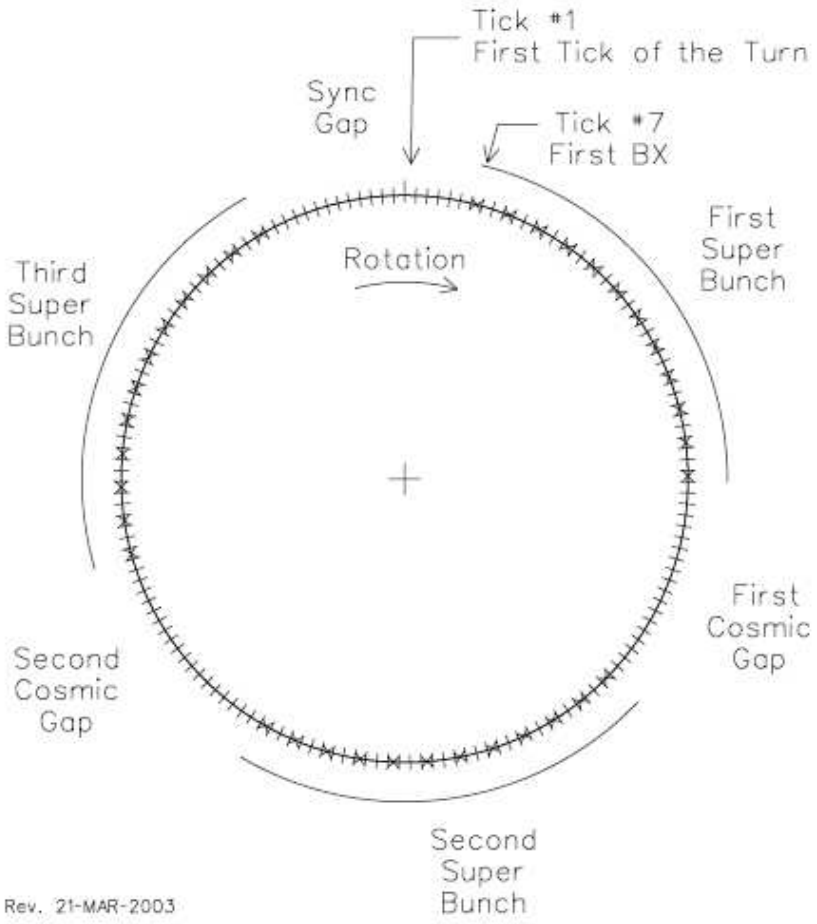

Figure 25: The Tevatron bunch structure. (Thanks to Dan Edmunds.)

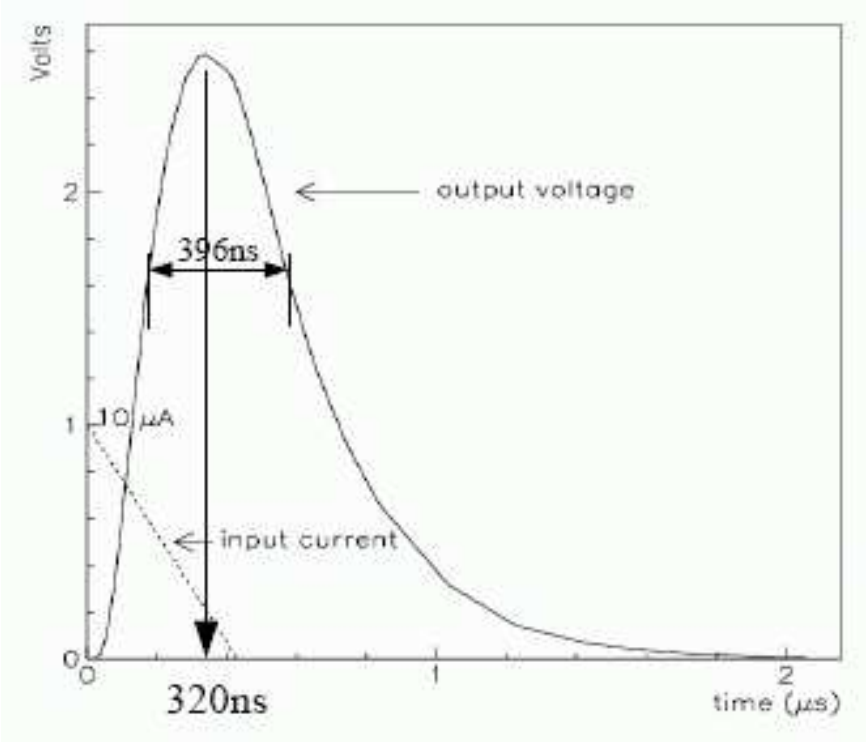

Figure 26: The timing of the calorimeter readout.

loss to the signal, it is more accurate to reduce the average jet energy by the appropriate amount, since most jets from higher-mass gluinos will still be above the jet energy threshold. Those from lower-mass gluinos that would then fall outside the threshold will not be included in the jet energy range studied, which is cut off again at 90 GeV.

10 Systematic Errors

Several sources of systematic errors have been identified. They fall into two general categories: errors affecting the calculation of signal acceptance and those that affect the number of estimated background events. The errors from all sources which affect the signal acceptance are added in quadrature. Table 3 shows the sources of uncertainty, and their total.

The first signal acceptance uncertainty is due to the modeling of the signal by the MC simulation. The error on the shift in average shower energy caused by the out-of-time calorimeter signals will be taken as 30% relative, equal to a $\pm 5\%$ absolute energy shift. Varying the jet energy within the data/MC jet energy scale uncertainty or this 5% shift from the out-of-time signals, changes the total efficiency by 3-7%, depending on the signal sample. Most jets are well above the 90 GeV energy threshold. Also, shifting the energy scale causes nearly as many jets to fall below the lower window cut as below the upper window cut (see below for a description of the window cut for signal selection). Varying the $|\eta|$ cut by ± 0.1 changed the efficiency by 9%. The total uncertainty from the MC modeling was estimated to be 20%, since other sources of

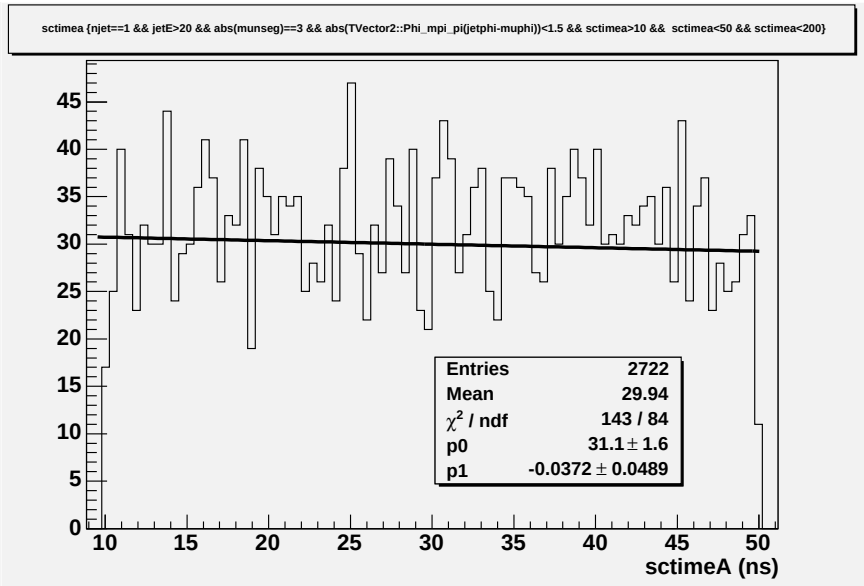

Figure 27: The number of muon showers above threshold vs. the muon scintillator time.

Source	Uncertainty
Geometrical/Kinematic Acceptance	0.2
Min-bias Overlap	0.15
Total	0.25

Table 3: The systematic uncertainties on signal efficiency, and their total (added in quadrature).

uncertainty (due to jet shape, for instance) could also contribute.

Another signal acceptance uncertainty is the efficiency due to the GAPSN trigger requirement, which was estimated to be 15%. See section 9 for more details.

There is a statistical error associated with the uncertainty in the normalization of the background, equal to 10%.

11 Results

If we apply the measured P_{nomu} to the wide-jet cosmic-muon data sample, we can estimate the energy spectrum of the expected wide-jet no-muon background, as shown in Figures 28 and 29 along with the observed wide-jet no-muon events in data. The estimated background predicts the data well, and there is little excess in data at any energy range, as seen in Figure 30, where the expected background has been subtracted from the data.

Given an observed number of candidate events, an expected number of background events, and a signal efficiency in a certain jet energy bin, we can exclude at 95%

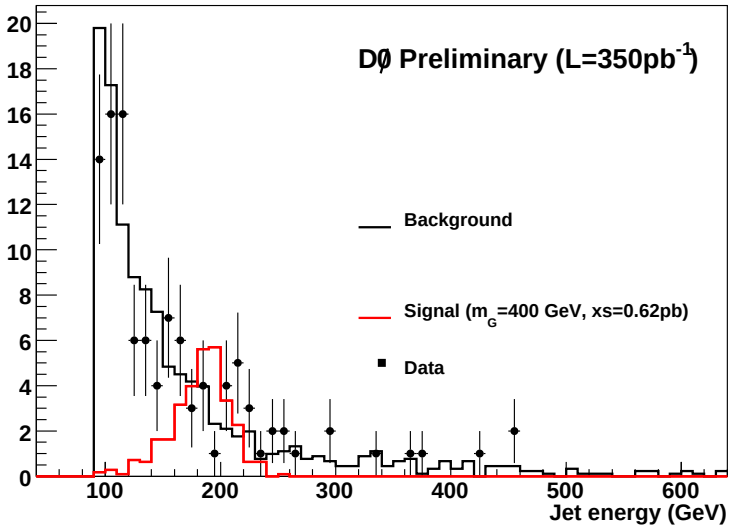

Figure 28: A comparison of the wide-jet no-muon data to the expected background. Also shown is the signal simulated for m_G=400 GeV and m_{LSP}=90 GeV at the excluded limit of 0.7 pb (in red).

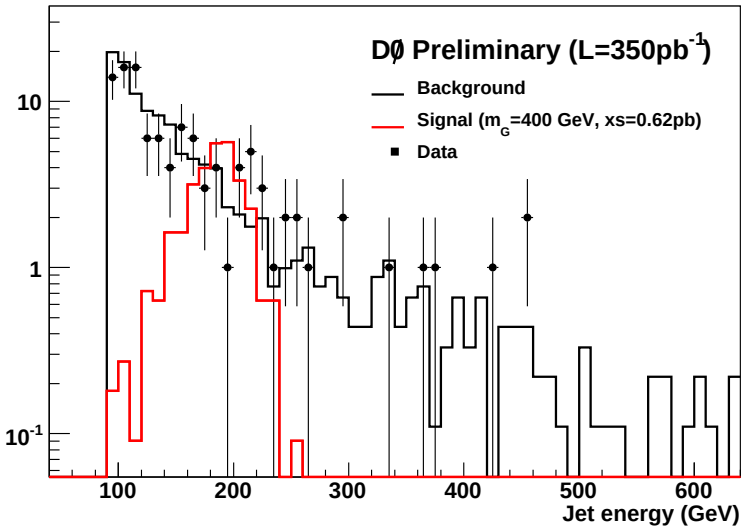

Figure 29: A comparison of the wide-jet no-muon data to the expected background, with log scale. Also shown is the signal simulated for m_G=400 GeV and m_{LSP}=90 GeV at the excluded limit of 0.7 pb (in red).

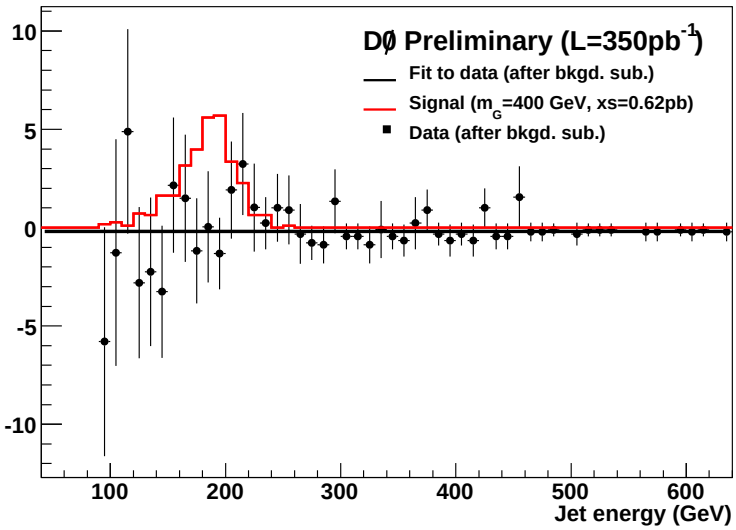

Figure 30: The wide-jet no-muon data, after subtracting the expected background. Also shown is the signal simulated for m_G=400 GeV and m_{LSP}=90 GeV at the excluded limit of 0.7 pb (in red).

C.L. a calculated rate of signal events giving jets of that energy, taking systematic uncertainties into account [8]. This is a fairly model-independent result, limiting the rate of any out-of-time mono-jet signal of a given energy. From there we can derive limits in the plane of $M_g - M_{LSP}$ for the stopped gluino model specifically.

The jet energy ranges chosen are calculated from the resolution of the simulated MC samples. The signal window for each of the four samples is from M-0.5*RMS – M+2.0*RMS, where M is the sample's jet energy mean (after all selections) and RMS is the sample's jet energies' RMS. Approximately 80% of the simulated signal events fell within this window cut, depending weakly on the signal mass. An asymmetric window was chosen since the background is falling exponentially with increasing jet energy, whereas the signal is roughly symmetric in jet energy around the mean. Table 4 shows, for each jet energy range considered, the number of events observed in data, expected from background, the signal efficiency, and the corresponding observed and expected [9] cross-section limits on signal jets. The integrated luminosity assumed was 350±20 pb^{-1}. These results are also shown in Figure 31.

From the relation between the gluino and LSP masses and the observed jet energy, Equation 1, one can solve for the gluino mass:

$$M_g = E + \sqrt{E^2 + M_{LSP}^2} \tag{2}$$

Using this equation, results can be translated from the generated set of signal samples

[8] The Bayesian limit setting routing "CL95" in the CVS package "limit_calculators" has been used.

[9] The expected limit is calculated by setting the number of "observed" events to the number of expected events from background. It is the limit that would be derived in the average experiment if there were no signal.

Jet E Range (GeV)	Data	Bgnd.	Eff.	Exp. Limit (pb)	Obs. Limit (pb)
94.6-111.6	46	48.18	0.05	1.39	1.27
126.8-171.8	32	37.84	0.10	0.59	0.45
169.3-233.8	27	21.56	0.11	0.40	0.62
214.2-286.6	14	9.57	0.10	0.30	0.52

Table 4: The data, background, efficiency, and observed and expected limits (at 95% C.L.) for each jet energy range.

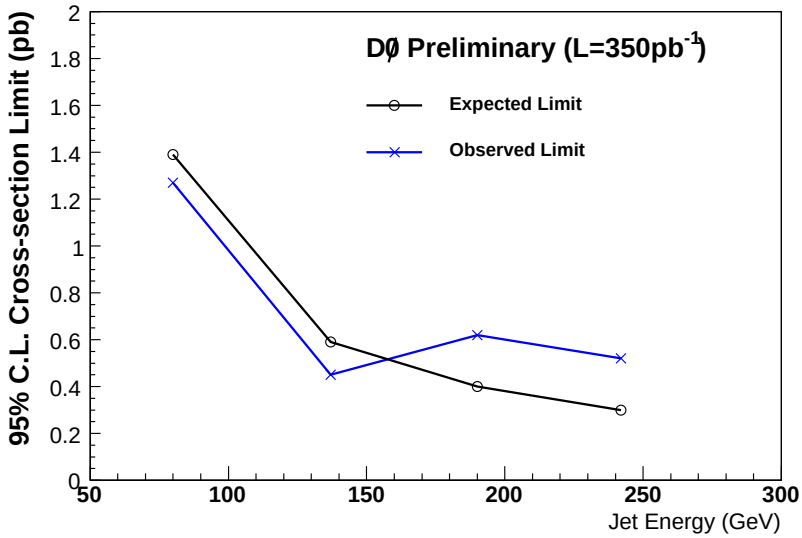

Figure 31: The 95% C.L. upper limits expected (black, open circles) and observed (blue, filled circles) on the cross-section of stopped particles decaying into a jet within various energy ranges.

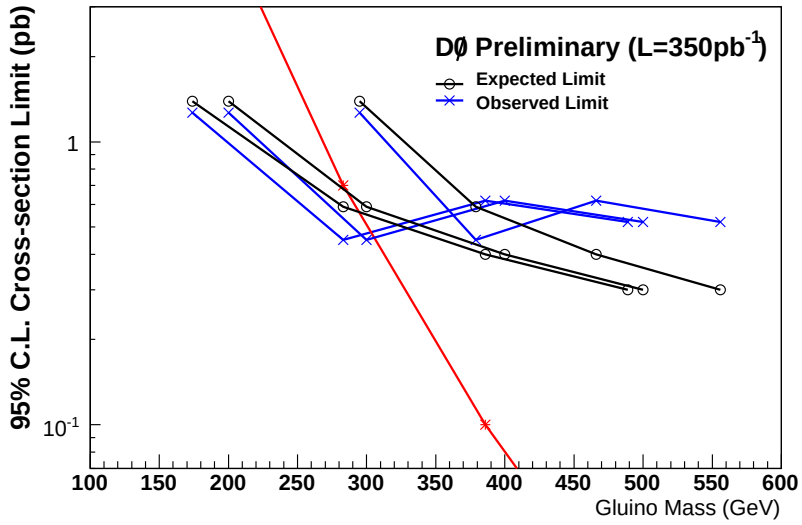

Figure 32: The 95% C.L. upper limits expected (black, open circles) and observed (blue, crosses) on the cross-section of stopped gluinos decaying into a jet. Also shown is the theoretical cross-section (red, stars), from [3].

to any other set of (M_g,M_{LSP}) which would give the same generated parton (jet) energy. For example, one of the generated samples had M_g=400 GeV and M_{LSP}=90 GeV (all of the generated samples had M_{LSP}=90 GeV, which corresponds to the Z mass). This corresponded to a parton (jet) energy of 190 GeV, as given by Equation 1. If instead M_{LSP} had been chosen to be 200 GeV, an equivalent jet energy could have been simulated by having M_g be 466 GeV, according to Equation 2. We can now place upper limits on the stopped gluino cross-section for a given LSP mass. These can be compared with the predicted cross-sections for stopped gluinos (which includes its production and its probability to stop) taken from [3]. Tables 5, 6, and 7 show the gluino cross-sections excluded for assumed LSP masses of 50, 90, and 200 GeV, respectively. These results are also shown in Figure 32.

Jet E (GeV)	Gluino Mass (GeV)	Observed Limit (pb)	Theoretical CS (pb)
80	174	1.27	10
137	283	0.45	0.7
190	386	0.62	0.1
242	489	0.52	0.02

Table 5: The gluino mass, observed cross-section limit, and the theoretical cross-section for each jet energy, assuming an LSP mass of 50 GeV.

Jet E (GeV)	Gluino Mass (GeV)	Observed Limit (pb)	Theoretical CS (pb)
80	200	1.27	5
137	300	.45	.5
190	400	.62	.05
242	500	.52	.01

Table 6: The gluino mass, observed cross-section limit, and the theoretical cross-section for each jet energy, assuming an LSP mass of 90 GeV.

Jet E (GeV)	Gluino Mass (GeV)	Observed Limit (pb)	Theoretical CS (pb)
80	295	1.27	.5
137	379	.45	.07
190	466	.62	.03
242	556	.52	.005

Table 7: The gluino mass, observed cross-section limit, and the theoretical cross-section for each jet energy, assuming an LSP mass of 200 GeV.

12 Discussion

This is the first experimental study for this type of signal at a hadron collider. The results from 350pb^{-1} of Tevatron data are not able to exclude a very large gluino mass. But the experience gained with the analysis methods and backgrounds involved allow us to have a good feel for the prospects of the stopped gluino search (or discovery!) in the future, both at the Tevatron with additional luminosity and at the nearly completed LHC, due to begin operation in 2007.

12.1 Extrapolation to Higher Integrated Luminosity

Assuming that no deviation is observed between the data and the expected background in the future, the 95% C.L. limits which could be set given additional luminosity can be predicted. One complication though is that the GAPSN triggers will become increasingly inefficient at higher instantaneous luminosities due to the increased probability of an overlapping min-bias interaction in an event during the gluino decay. However, since only the higher energy gluino decays will be of interest (because the lower energy decays have been excluded), the JT_125TT trigger will be efficient by itself. There has also been effort to include a trigger during the "cosmic gaps" in the beam bunch structure, which would add an additional 20% trigger efficiency. Thus, it is safe to assume that overall trigger efficiency can remain at least as high as for this first analysis.

With 2fb^{-1}...

12.2 Comments on this Search at the LHC

The LHC will produce many more stopped gluinos...

References

[1] N. Arkani-Hamed, S. Dimopoulos, G. F. Giudice and A. Romanino, Nucl. Phys. B **709**, 3 (2005) [arXiv:hep-ph/0409232].

[2] A. C. Kraan, Eur. Phys. J. C **37**, 91 (2004) [arXiv:hep-ex/0404001].

[3] A. Arvanitaki, S. Dimopoulos, A. Pierce, S. Rajendran and J. Wacker, arXiv:hep-ph/0506242.

[4] G. C. Blazey *et al.*, in *Proceedings of the Workshop: "QCD and Weak Boson Physics in Run II,"* edited by U. Baur, R. K. Ellis, and D. Zeppenfeld, (Fermilab, Batavia, IL, 2000) p. 47; see Sec. 3.5 for details.

13 Thanks

This work was motivated by the phenomenological studies of Jay Wacker, et al. from Stanford. He was also very helpful in discussing various theoretical issues related to this work. I also thank Dean Schamberger, Dan Edmunds, Gustaaf Brooijmans, John Parsons, and Terry Wyatt for their help, input, and support.